ARTICLE OPEN

Check for updates

Deletion of *Crtc1* leads to hippocampal neuroenergetic impairments associated with depressive-like behavior

Antoine Cherix[1,2]✉, Carole Poitry-Yamate[3], Bernard Lanz[1], Olivia Zanoletti[4], Jocelyn Grosse[4], Carmen Sandi[4], Rolf Gruetter[1] and Jean-René Cardinaux[2]✉

Mood disorders (MD) are a major burden on society as their biology remains poorly understood, challenging both diagnosis and therapy. Among many observed biological dysfunctions, homeostatic dysregulation, such as metabolic syndrome (MeS), shows considerable comorbidity with MD. Recently, CREB-regulated transcription coactivator 1 (CRTC1), a regulator of brain metabolism, was proposed as a promising factor to understand this relationship. Searching for imaging biomarkers and associating them with pathophysiological mechanisms using preclinical models can provide significant insight into these complex psychiatric diseases and help the development of personalized healthcare. Here, we used neuroimaging technologies to show that deletion of *Crtc1* in mice leads to an imaging fingerprint of hippocampal metabolic impairment related to depressive-like behavior. By identifying a deficiency in hippocampal glucose metabolism as the underlying molecular/physiological origin of the markers, we could assign an energy-boosting mood-stabilizing treatment, ebselen, which rescued behavior and neuroimaging markers. Finally, our results point toward the GABAergic system as a potential therapeutic target for behavioral dysfunctions related to metabolic disorders. This study provides new insights on *Crtc1's* and MeS's relationship to MD and establishes depression-related markers with clinical potential.

Molecular Psychiatry (2022) 27:4485–4501; https://doi.org/10.1038/s41380-022-01791-5

INTRODUCTION

Mood disorders (MD) are among the leading causes of disability worldwide [1, 2]. The difficulty in defining appropriate treatments relates to the fact that these complex, dynamic and multifactorial psychiatric diseases are poorly understood [3]. The way these diseases are approached complicates the identification of therapeutic targets: diagnosis is currently based on subjective signs and symptoms, rather than on objective biological or chemical measurements. In practice, there is an urgency to establish reliable biomarkers within a framework of personalized treatment approaches [4, 5]. Neuroimaging techniques, such as magnetic resonance imaging (MRI), spectroscopy (MRS) and positron emission tomography (PET) are promising tools to achieve this goal by providing brain-specific information [6]. Nevertheless, development and validation of neuroimaging markers for psychiatry require prior understanding of their underlying pathophysiological origin and the genetic and environmental factors linking these markers to the behavioral deficit [6]. Among many potential etiological factors that have been identified, metabolic syndrome (MeS), i.e., a combination of obesity, dyslipidemia, insulin resistance, and hypertension, has gained significant attention due to its high co-occurrence with MD [7–10]. However, the mechanisms and the causality relationship between peripheral metabolic alterations and dysfunction of the central mood regulation, and how this translates to in vivo brain measurements, remain to be fully elucidated.

The CREB-Regulated Transcription Coactivator 1 (CRTC1) gene has emerged as a promising target to study how features of MeS can lead to behavioral impairments. Several studies have identified a relationship between CRTC1 polymorphisms and psychiatric disorders, with focus on obesity parameters [11–14] and stress [15]. Through its enhancement of CREB transcriptional activity and because of its ability to sense both Ca^{2+} and cAMP second messengers in neurons, CRTC1 has been established as a key regulator of brain function and metabolism [16, 17]. CRTC1 is involved in synaptic plasticity and memory formation [18–20] and participates in the regulation of energy and mood balance [21, 22]. Importantly, CRTC1 has been implicated in rodent depressive-like behavior [23–26], which can be triggered by excessive CRTC1 phosphorylation and cytoplasmic sequestration as a response to chronic stress [27]. Thus, the *Crtc1* knock-out ($Crtc1^{-/-}$) mouse was shown to be a useful model to study the pathways and mechanisms linking metabolic diseases with depression [21, 22, 28, 29] and to understand associated resistance to classic antidepressants, in particular to fluoxetine [30, 31].

[1]Laboratory for Functional and Metabolic Imaging (LIFMET), École Polytechnique Fédérale de Lausanne (EPFL), Lausanne, Switzerland. [2]Center for Psychiatric Neuroscience and Service of Child and Adolescent Psychiatry, Department of Psychiatry, Lausanne University Hospital and University of Lausanne, Prilly-Lausanne, Switzerland. [3]Animal Imaging and Technology (AIT), Center for Biomedical Imaging (CIBM), École Polytechnique Fédérale de Lausanne (EPFL), Lausanne, Switzerland. [4]Laboratory of Behavioral Genetics, Brain and Mind Institute, School of Life Sciences, École Polytechnique Fédérale de Lausanne (EPFL), Lausanne, Switzerland. ✉email: antoine.cherix@ndcn.ox.ac.uk; jean-rene.cardinaux@chuv.ch

Received: 9 March 2021 Revised: 8 September 2022 Accepted: 9 September 2022
Published online: 12 October 2022

Here, using state-of-the-art preclinical neuroimaging technologies, we sought to identify fingerprints of brain metabolic disturbances in *Crtc1*$^{-/-}$ mice and to explore their mechanistic relationship with behavioral dysfunctions and MeS. By combining MRS, MRI and PET, we found that deletion of *Crtc1* in mice uncovers hippocampal neuroenergetic markers that are associated with depressive-like behavior. By deciphering the pathophysiological mechanisms associated with these brain markers and behavior, we were able to select a targeted treatment, which reversed the pathological phenotype. Our results highlight new mechanisms linking *Crtc1* and MeS with the development of depressive-like behavior, bringing to the forefront associated preclinical neuroimaging markers with clinical potential, and identification of a compatible mood-stabilizer with therapeutic capacity.

MATERIALS AND METHODS

Animals

Crtc1 knock-out (*Crtc1*$^{-/-}$) mice and wild-type (WT, i.e., *Crtc1*$^{+/+}$) littermates were bred and genotyped as previously described [30]. Mice were housed in standard Plexiglass filter-top cages in a normal 12 h daylight cycle environment at a temperature of 23 ± 1 °C and humidity of 40%. Animals had ad libitum access to standard rodent chow diet and water. Weaning of newborn mice was done at 21 days and followed by group-housing until being isolated at ~6 weeks to prevent injuries of cage mates induced by the aggressive *Crtc1*$^{-/-}$ male mice [30]. All experiments were carried out with the approval of the Cantonal Veterinary Authorities (Vaud, Switzerland) and conducted according to the Federal and Local ethical guidelines of Switzerland (Service de la consommation et des affaires vétérinaires, Epalinges, Switzerland) in compliance with the ARRIVE (Animal Research: Reporting in vivo Experiments) guidelines.

Experimental design

Three sets of experimental designs of the present study in male *Crtc1*$^{-/-}$ and WT mice were implemented (sample sizes estimated from previous studies). In the first experimental set, basal metabolic function was assessed and quantified in *Crtc1*$^{-/-}$ and WT mice at the age of 6 weeks postnatal, and prior to the social separation from their littermates. The second experimental set was performed, longitudinally for 18 weeks, in mice aged from 6 to 24 weeks postnatal. As before, the first measurement time point was at 6 weeks of age; thereafter, animals were socially isolated until the end of the study in an enriched environment that included a paper house and a wooden stick. The third set of experiments was conducted for 4 weeks, in mice aged from 6 to 10 weeks postnatal. Animals were socially isolated again after the first imaging time point and were then subjected to a 4 weeks stress and treatment (randomly assigned and blinded) protocol.

In vivo ^{1}H-magnetic resonance spectroscopy (^{1}H-MRS)

Localized in vivo ^{1}H-magnetic resonance spectroscopy (^{1}H-MRS) was performed in the dorsal hippocampus (DH) and cingulate prefrontal cortex (PFC) of *Crtc1*$^{-/-}$ and WT mice. Animals were maintained under continuous isoflurane anesthesia (1.5% mixed with 1:1 air:oxygen mixture) and monitoring of physiology during the entire scan for physiological parameters. Breathing rate per minute was maintained between 70–100 rpm using a small animal monitor (SA Instruments Inc., New York, USA) and rectal temperature was kept at 36.5 ± 0.4 °C with a circulating heating water bath and assessed using a temperature rectal probe. Animals were scanned in a horizontal 14.1 T/26 cm Varian magnet (Agilent Inc., USA) with a homemade transceiver ^{1}H surface coil in quadrature. A set of T_2-weighed images was acquired using a fast spin echo sequence (15 × 0.4 mm slices, TE_{eff}/TR = 50/2000 ms, averages 2) to localize the volume of interest (VOI). The voxels were positioned to include either a single DH (1 × 2 × 1 mm^3) or PFC (1.4 × 1.6 × 1.2 mm^3). In each voxel, the field homogeneity was adjusted using FAST(EST)MAP [32] to reach a typical water linewidth of 15 ± 1 Hz for DH and 14 ± 1 Hz for PFC. Proton spectra were acquired with a spin echo full intensity acquired localized (SPECIAL) sequence (TE/TR = 2.8/4000 ms) [33] using VAPOR water suppression and outer volume suppression. Scans were acquired in blocks of 30 times 16 averages for DH and 8 averages for PFC. Post processing included frequency correction based on the creatine peak and summing of all the spectra before quantification with LCModel [34]. The water signal was used as internal reference and fitting quality was assessed using Cramer-Rao lower bounds errors (CRLB) for a typical rejection threshold of CRLB + 2 × SD [35]. ^{1}H-MRS acquisitions from DH and PFC of *Crtc1*$^{-/-}$ mice and their WT littermates led to the reliable quantification of up to 20 individual metabolites, with a comparable spectra quality for both groups, i.e., with a signal-to-noise ratio (SNR) of 11.8 ± 0.9 for WT vs. 13.4 ± 1.3 for *Crtc1*$^{-/-}$ in DH, and 15.0 ± 0.7 for WT vs. 15.7 ± 1.0 for *Crtc1*$^{-/-}$ in PFC. MRI images acquired were used to quantify PFC volume using a pattern-based morphometric approach. A surface in the shape of a kite was drawn on the coronal images with each corner situated between the major sulcus, the central lower part of the corpus callosum and the two cingulum bundles as reference points. The surface was quantified using ImageJ and averaged over the group for each brain section.

High-resolution NMR spectroscopy

Mice were sacrificed using a microwave fixation apparatus (Gerling Applied Engineering Inc., Modesto, CA, USA) at 4 kW for 0.6 s after intraperitoneal injection of a lethal dose of sodium pentobarbital (~50 µl to reach a dose of 150 mg/kg). Brain was extracted, DH was removed, frozen on liquid nitrogen and stored at −80 °C. Samples were then ground on mortar using liquid nitrogen, weighed and followed by a $CHCl_3$/MeOH Folch-Pi extraction [36, 37]. Samples were stirred at 4 °C in a 1:1:1 mixture of $CHCl_3$:MeOH:H_2O for 30 min after what the aqueous phase was collected and lyophilized. The resulting extracted metabolites were resuspended in 600 µl deuterium oxide containing 0.1 µM 4,4-dimethyl-4-silapentane-1-sulfonic acid (DSS) as internal reference. High-resolution NMR was performed using a DRX-600 spectrometer (Bruker BioSpin, Fällanden, Switzerland). Proton-NMR (^{1}H-NMR) spectra were acquired with 400 scans using a pulse-acquired sequence (flip angle 30° and 5 s pulse delay). Phosphorous-NMR (^{31}P-NMR) spectra were acquired on the same sample with 10,000 scans using a proton-decoupled pulse-acquired sequence (flip angle 90° and 5 s pulse delay). Spectra were analyzed and quantified using the MestReNova software (Mestrelab Research, Santiagio de Compostela, Spain). Spectra were phase and baseline corrected manually. Afterwards, peaks were integrated and referenced to the DSS resonance and normalized to NAA. NAA concentration in DH was assumed to be 7 mM as measured in vivo. The following resonance (δ, in ppm) were considered (number of protons, spectral pattern): AXP (sum of AMP, ADP and ATP) δ 6.13 (1H, d), creatine δ 3.026 (3H, s), phosphocreatine δ 3.028 (3H, s) and N-acetyl-aspartate δ 2.00 (1H, s). The following resonance were integrated in the ^{31}P spectrum after setting the PCr resonance to 0 ppm: NAD^+ δ −8.31 (2P, q), NADH δ −8.15 (2P, m), UDPGlc δ −9.83 (2P, m), P_i δ 3.8 (1P, m), GPC δ 3.07 (1P, s). The spectral pattern is described as follows: s, singlet; d, doublet; t, triplet; dd, doublet of doublet; m, multiplet. Due to overlap between resonances, the NADH/NAD^+ ratio was calculated as follows: the left part of the NAD^+ quadruplet (X = 2·NADH + NAD^+ + UDPGlc) was integrated as well as the right part of the quadruplet (Y = NAD^+) and the −9.83 ppm UDPGlc resonance (Z = UDPGlc). Then, NADH was obtained by subtracting Y and Z from X, followed by a division by 2. As we did not see changes in GPC in the hippocampus between groups, we used this signal as an internal reference for ^{13}P-NMR spectra quantification.

In vivo ^{18}FDG positron emission tomography (^{18}FDG-PET)

Dynamic non-invasive fluorodeoxyglucose positron emission tomography (^{18}FDG-PET) was performed as described previously [38, 39]. Briefly, mice under 1–2% (vol/vol) isoflurane anesthesia in O_2 were positioned in the scanner after tail vein cannulation and remained monitored for temperature and breathing rate throughout the experiment. Imaging was performed after i.v. bolus injection of ^{18}FDG (~50 MBq) through the tail vein catheter within the first 20 s of a 50 min duration PET scan. After histogramming and image reconstruction with the Labpet software (Gamma Medica, Sherbrook, Canada), PMOD 2.95 software (PMOD Technologies, Zurich) was used for the determination of the heat-maps of standardized uptake value, defined as (mean ROI activity [kBq/cm^3])/(injected dose [kBq]/body weight [g]). Regions of interest, i.e., hippocampus (2 × 5.5 mm^2), were manually drawn over one axial slice. Mathematical modeling of hippocampal glucose metabolism was performed as previously described [38, 39], using the radioactive decay-corrected activity density values in [kBq/cc]. Intergroup differences could not be attributed to differences in the amount of ^{18}FDG entering the blood, body weight, nor to differences in the kinetics of the arterial input function.

Gene expression analysis

Total RNA was extracted and purified from micropunches of DH using a RNeasy Plus Minikit (Qiagen, Venolo, Netherland) according to the manufacturer's instructions. NanoDrop Lite (Thermo Scientific, Wilmington, DE, USA) was used for the UV spectrophotometric quantification of RNA concentrations and purity assessment. cDNAs were obtained by reverse transcription of the mRNA samples in 50µl reaction using Taqman Reagents and random hexamers (Applied Biosystems, Foster City, CA, USA). Real-time quantitative PCR was subsequently performed with cDNA concentrations of 0.16 ng/µl on a 96-well plate with SYBR Green PCR Master Mix (Applied Biosystems). The reaction started with a 2 min step at 50 °C and 10 min at 95 °C, followed by 45 cycles of 15 s at 95 °C and 1 min at 60 °C, and 30 s elongation at 72 °C. The relative gene expression was determined using the comparative ΔΔCt method and normalized to β-actine and β2 microglobulin (β-2m) as housekeeping genes. The primers were used at a concentration of 250 nM and described in Supplementary Table 1.

Mitochondrial respirometry

Animals were sacrificed by rapid decapitation followed by DH dissection. The tissue was weighed, placed in a petri dish on ice with 2 ml of relaxing solution (2.8 mM Ca_2K_2EGTA, 7.2 mM K_2EGTA, 5.8 mM ATP, 6.6 mM $MgCl_2$, 20 mM taurine, 15 mM phosphocreatine, 20 mM imidazole, 0.5 mM dithiothreitol and 50 mM MES, pH = 7.1) until further preparation. Gentle homogenization was then performed in ice-cold respirometry medium (miR05: 0.5 mM EGTA, 3 mM $MgCl_2$, 60 mM potassium lactobionate, 20 mM taurine, 10 mM KH_2PO_4, 20 mM HEPED, 110 mM sucrose and 0.1% (w/v) BSA, pH = 7.1) with an Eppendorf pestle. Two mg of tissue were then used for high-resolution respirometry (Oroboros Oxygraph 2K, Oroboros Instruments, Innsbruck, Austria) to measure mitochondrial respiration rates at 37 °C. The experimental protocol consists in several experimental steps, which test the capacity of the different mitochondrial electron transport chain components by measuring the O_2 flux in the sample. (1) The activity of complex I (CI) is measured by adding ADP (5 mM) to a mixture of malate (2 mM), pyruvate (10 mM) and glutamate (20 mM). (2) Succinate (10 mM) is subsequently added to the medium to stimulate complex II and measure the capacity of both complexes (CI + CII). (3) Protonophore FCCP (carbonyl cyanide 4-(trifluoromethoxy)phenylhydrazone) is then used (successive titrations of 0.2 µM until reaching maximal respiration) to uncouple the respiration and provides information on the maximal capacity of the electron transfer system (ETS). (4) Rotenone (0.1 µM) was then used to inhibit complex I and quantify the contribution of complex II in the uncoupled sate (ETS CII). (5) Antimycin (2 µM) is added to inhibit complex III and block the ETS in order to assess the residual oxygen consumption (ROX) provided by oxidative reactions unrelated to mitochondrial respiration. Oxygen fluxes were normalized by the wet weight of tissue sample and corrected for ROX.

Blood metabolite measurements

Blood sampling was performed after the last ^{1}H-MRS scan of the longitudinal and treatment studies. Blood was collected from the trunk after head decapitation using collection tubes (Heparin/Li^+ Microvette CB300 LH, Sarstedt). Samples were centrifugated at 1000 × *g* for 10 min at room temperature leading to ~100 µl of plasma, which was then frozen in liquid nitrogen and stored at −80 °C. Blood MeS markers were then quantified using an ELISA kit (insulin: EZRMI-13K, Millipore; glucose) and colorimetric assays (triglyceride: 10010303, Cayman;: 10009582, Cayman) according to the manufacturer's instructions and with the following dilution factors: triglyceride: 1/2, insulin: 1/5, and glucose: 1/20.

Open field test (OF)

The open-field test was used to assess mice locomotor activity [40]. Animals were placed in a white arena (50 × 50 × 40 m^3) illuminated with dimmed light (30lux). After 30 min of habituation in the experiment room, mice were transferred to the center of the arena and were allowed to explore for 25 min. Mice were tracked for 20 min using a tracking software (Ethovision 11.0 XT, Noldus, Information Technology), after removing the habituation period of the 5 first minutes in each video. An analysis of these videos provided the mean distance traveled and mean velocity.

Porsolt forced swim test (FST)

Animals were introduced into a 5 l capacity cylinder of 15 cm in diameter containing 23–25 °C tap water in dimmed light (30lux) as described in Breuillaud et al. [30]. Water level in the cylinder was set to prevent the mouse from touching the bottom of the enclosure or to avoid any possible escape. The session was recorded with a camera positioned on top of the setup for 6 min and videos were analyzed using a tracking software (Ethovision 11.0 XT, Noldus, Information Technology). Immobility time was measured after discarding the first minute of swimming in each video.

Tail suspension test (TST)

Mice were suspended individually by the tail on a metal bar at a height of ~35 cm. A stripe of adhesive tape was attached to the mouse tail at ~2 cm from the extremity to perform the suspension to the bar. Animals were videotaped from the side of the setup and immobility time was recorded manually during 5 min [30].

Composite behavior (averaged *z*-scores)

In the longitudinal study, a composite behavior was computed and considered both immobility times from the FST and TST reflecting animal's behavioral despair. A *z*-score was calculated using MATLAB (Version 9.6, The MathsWorks Inc, Natick, MA) for each mouse and time-point using MATLAB function *normalize* with the option argument *zscore*. The *z*-score was computed using the overall average and standard deviation (including all mice and time-points). Finally, the behavioral composite *z*-score was calculated by averaging the two *z*-scores of TST and FST for each mouse time point.

Repeated open-space forced swim test (OSFST)

The repeated OSFST protocol was used as described previously [30, 31]. Animals were introduced into a cage (45 × 28 × 20 cm) filled up to ~13 cm with 34–35 °C tap water colored with milk. Mice were subjected to 4 consecutive days of swimming (day −9 to −6) for 15 min. Mice were then subjected to additional swim sessions for 3 weeks under treatment, according to the following interval: days −1, 3, 7, 10, 13, 17, 20. Water was replaced regularly between tests to ensure constant water temperature. Animals were videotaped from above and immobility time was recorded manually.

Ebselen treatment

Animals were treated with ebselen (Tokyo Chemical Industry, Tokyo, Japan) starting from day 0 until the end of the repeated OSFST protocol. Mice received oral administration (gavage) of ebselen (10 mg/kg) dissolved in 5% (w/v) carboxymethylcellulose (CMC; Sigma Aldrich) two times a day (mornings and evenings) for 21 consecutive days. The control group was administered a 5% CMC vehicle solution of the same volume. The dose was adjusted to any body weight gain.

Neuroimaging marker assessment

Receiver operating characteristic (ROC) curves and the area under the ROC curve (AUC) were established for discriminating *Crtc1*$^{-/-}$ from WT mice on the basis of their PFC alterations, which took into account the concentration of total choline (tCho) and tissue volume separately or as an average of individual *z*-scores. For this averaged score, the PFC individual *z*-scores were calculated using the whole sample average and standard deviation for both experiments combined (longitudinal and treatment). ROC curves and AUC were also established for the neuroenergetic profile (Lac and PCr) of DH for discriminating mice with "high" and "low" depressive-like behavior. In order to consider the different ways of assessing the behavior between the longitudinal (FST + TST) and treatment (OSFST) studies, a behavioral *z*-scores was calculated using the sample average and standard deviation for each behavioral test separately. Subsequently, mice were separated into "high" or "low" depressive-like behavior, whether their score was higher (+z) or lower (−z) than the average, respectively. The ability of the DH neuroimaging markers to distinguish these two populations was tested using ROC curves for either Lac or PCr concentrations separately or as an average of individual *z*-scores.

In vivo indirect ^{13}C magnetic resonance spectroscopy (^{1}H-[^{13}C]-MRS)

Non-invasive indirect carbon-13 magnetic resonance spectroscopy (^{1}H-[^{13}C]-MRS) was performed as previously described [39, 41]. The experimental set-up was comparable to that of ^{1}H-MRS, with two main differences (1) animals underwent femoral vein cannulation for the

infusion of uniformly labeled ^{13}C-glucose ([U-$^{13}C_6$]Glc) for a scan of ~230 min duration; and (2) the coil included a ^{13}C channel. Breathing rate was maintained at ~80 rpm and rectal body temperature was kept at 36.2 ± 0.3 °C for both groups throughout the scan. Blood glycemia was measured before (Glc_{Blood}(WT) = 7.7 ± 3.5 mM vs. Glc_{Blood}(*Crtc1*$^{-/-}$) = 7.3 ± 0.9 mM, n.s.) and after the infusion/scan (Glc_{Blood}(WT) = 21 ± 4 mM vs. Glc_{Blood}(*Crtc1*$^{-/-}$) = 28 ± 13 mM, n.s.) using a Breeze-2 meter (Bayer AG, Leverkusen, Germany). At the end of the experiment, blood lactate levels (Lac_{blood}(WT) = 7.7 ± 1.0 mM vs. Lac_{blood}(*Crtc1*$^{-/-}$) = 7.9 ± 0.9 mM; n.s.) were measured using two nearby GM7 analyzers (Analox Instruments Ltd, Stourbridge, UK). The VOI included the bilateral DH (2 × 5.5 × 1.5 mm^3) and led to a typical water linewidth of 20 ± 1 Hz after field homogeneity adjustment. ^{1}H-[^{13}C]-MRS spectra were acquired using the full intensity SPECIAL-BISEP sequence (TE = 2.8 ms, TR = 4000 ms, averages = 8) as

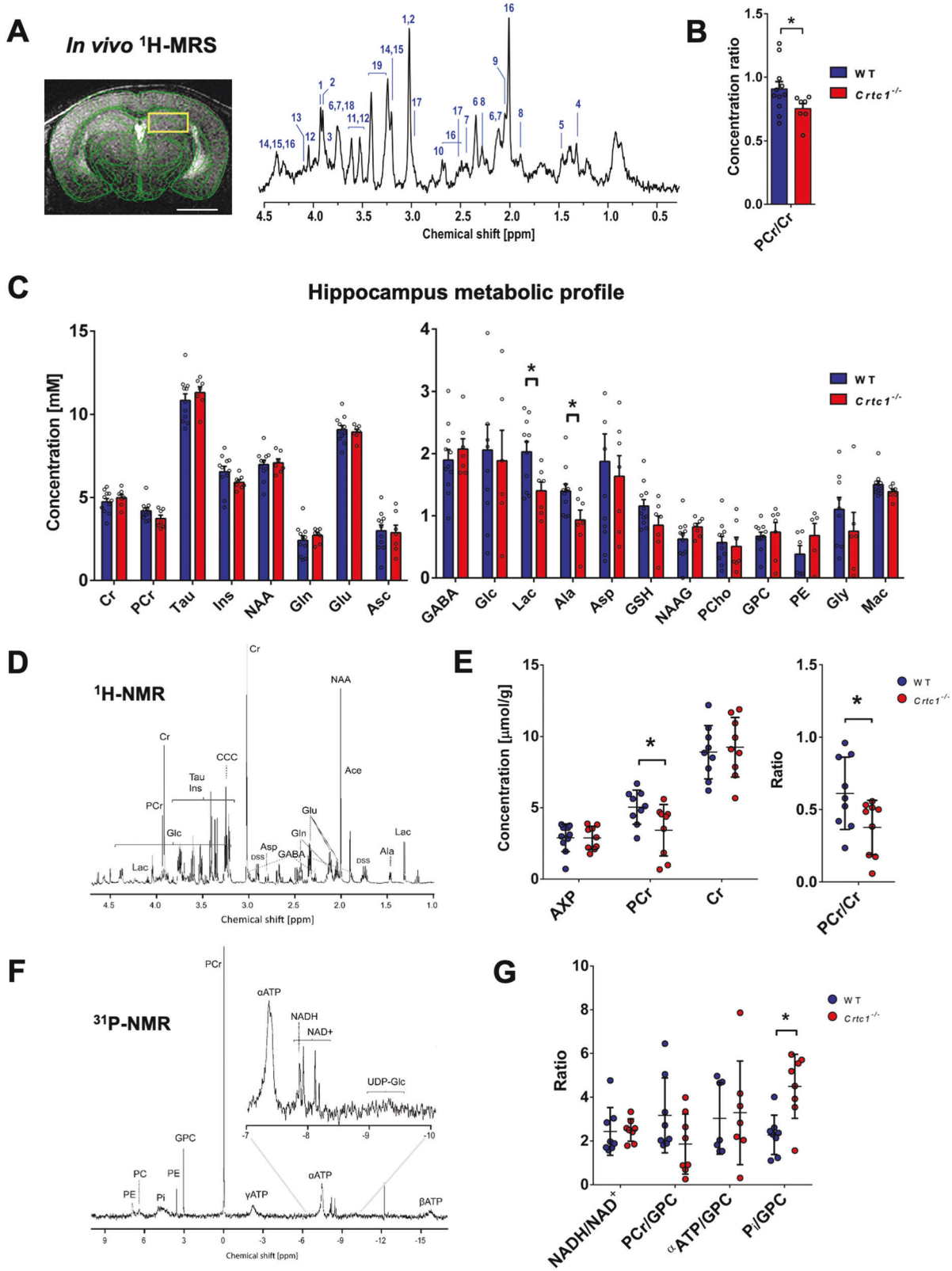

Fig. 1 Deletion of *Crtc1* is associated with a neuroimaging fingerprint of reduced hippocampal neuroenergetics. A T_2-weighted image acquired for localized MRS (VOI including dorsal hippocampus: yellow rectangle), with a scale bar of 2 mm (left) and typical ^{1}H-MRS spectrum acquired in the dorsal hippocampus (DH) of 6 weeks old mice at 14.1 Tesla (right). Metabolites in the spectrum include: 1. phosphocreatine (PCr), 2. creatine (Cr), 3. glucose (Glc), 4. lactate (Lac), 5. alanine (Ala), 6. glutamate (Glu), 7. glutamine (Gln), 8. γ-aminobutyric acid (GABA), 9. N-acetylaspartyl-glutamate (NAAG), 10. aspartate (Asp), 11. glycine (Gly), 12. myo-inositol (Ins), 13. phosphoethanolamine (PE), 14. glycerophosphorylcholine (GPC), 15. phosphorylcholine (PCho), 16. N-acetyl-aspartate (NAA), 17. glutathione (GSH), 18. ascorbate (Asc), 19. taurine (Tau) as well as macromolecules (mac). Spectrum is shown with 3Hz exponential apodization. **B**, **C** Quantification of DH neurochemical profile from ^{1}H-MRS in wild-type (WT; $n = 10$) and *Crtc1*$^{-/-}$ ($n = 6$) mice, *$p < 0.05$, unpaired Student's t test. Data are shown as mean ± s.e.m. **D** Typical high-resolution ^{1}H-NMR spectrum of DH extracts acquired at 600 MHz with **E** quantification of AXP (sum of AMP, ADP and ATP), PCr and Cr in wild-type ($n = 8$) and *Crtc1*$^{-/-}$ ($n = 8$) mice, *$p < 0.05$, Mann–Whitney test. **F** Typical high-resolution ^{31}P-NMR spectrum of DH extracts with **G** quantification of NADH/NAD$^+$ ratio as well as PCr, α-ATP and inorganic phosphate (P_i) relative to the GPC resonance in wild-type ($n = 8$) and *Crtc1*$^{-/-}$ ($n = 8$) mice, *$p < 0.05$, Mann–Whitney test. All high-resolution data (**E** and **G**) are shown as mean ± s.d.

previously described [39, 42, 43]. The non-edited (proton, ^{1}H) and inverted spectra (editing OFF and ON) were obtained using an interleaved acquisition and were subtracted in the post processing steps to obtain the edited spectra (protons bound to carbon 13, ^{1}H-[^{13}C]). The non-edited spectra were quantified using a standard basis set for the neurochemical profile, while the edited spectra were fitted with a basis set that included simulated LacC3, LacC2, AlaC2 + C3, GluC4, GluC3, GluC2, GlnC4, GlnC3, GlnC2, AspC3, AspC2, GABAC4, GABAC3, GABAC2 and acquired spectra of glucose. In vivo ^{1}H-[^{13}C]-MRS enables to follow the fate of brain glucose and its incorporation in several brain metabolites infusion of [U-$^{13}C_6$]Glc. Scanning the bilateral DH allowed us to quantify 12 metabolite resonances with a 10 min time resolution and a comparable SNR (as defined by the LCModel, i.e., the ratio of the maximum in the spectrum-minus-baseline to twice the rms residuals) between WT and *Crtc1*$^{-/-}$ mice (SNR(^{1}H): 21.4 ± 1.4 vs. 21.5 ± 0.8; SNR(^{1}H-[^{13}C]): 6.2 ± 0.5 vs. 5.6 ± 0.5, for WT and *Crtc1*$^{-/-}$ respectively, mean ± s.e.m). ^{13}C concentration curves of each metabolite were determined by multiplying the fractional enrichment (FE) with the total molecular concentration measured in the non-edited spectra. Mathematical modeling was performed using either a "1-compartment" or a "pseudo 3-compartment" model of brain energy metabolism (see Cherix et al. [39] for a complete description of the modeling). For both models, the cerebral metabolic rate of glucose (CMR_{Glc}) was set to the value obtained in the same voxel from the ^{18}FDG-PET experiments. Following fluxes were included in the 1-compartment model: tricarboxylic acid cycle (V_{TCA}); a dilution flux from blood lactate (V_{dil}^{in}) and from blood acetate (V_{dil}^{g}); a transmitochondrial flux (V_x); and finally, a neurotransmission flux (V_{NT}). The estimated fluxes from the pseudo 3-compartment model included: a dilution flux from blood lactate (V_{dil}^{in}) and from blood acetate (V_{dil}^{g}); the pyruvate dehydrogenase activity of excitatory (V_{PDH}^{e}) and inhibitory (V_{PDH}^{i}) neurons; a transmitochondrial flux for excitatory (V_x^{e}) and inhibitory (V_x^{i}) neurons; a neurotransmission flux for excitatory (V_{NT}^{e}) and inhibitory (V_{NT}^{i}) neurons; glutamate decarboxylase activity (V_{GAD}); and two exchange fluxes between two Gln or two GABA pools (V_{ex}^{g} and V_{ex}^{i}). Values of pyruvate carboxylase activity (V_{PC}), glial tricarboxylic acid cycle (V_g) and glial transmitochondrial flux (V_x^{g}) were fixed to known values and glial Gln efflux (V_{eff}) was set equal to V_{PC}, as described in Cherix et al. [39]. The other parameters were calculated from the estimated fluxes through mass-balance equations, assuming metabolic steady-state (i.e., no net change in metabolites concentration over the experiment duration): the GABA TCA shunt ($V_{shunt}^{i} = V_{GAD} - V_{NT}^{i}$), glutamine synthetase activity ($V_{GS} = V_{NT}^{e} - V_{NT}^{i} + V_{PC}$), total GABA TCA ($V_{TCA}^{i} = V_{PDH}^{i} + V_{shunt}^{i}$); total glial TCA ($V_{TCA}^{g} = V_g + V_{PC} + V_{NT}^{i}$), and the oxidative cerebral metabolic rate of glucose ($CMR_{Glc}(ox) = (V_{TCA}^{i} + V_{TCA}^{e} + V_{TCA}^{g} + V_{PC})/2$). The brain-to-blood lactate efflux was calculated ($V_{dil}^{out} = V_{dil}^{in} \cdot Lac_{brain}/Lac_{blood}$) using the lactate concentration measured in the hippocampus ($Lac_{brain}(WT) = 2.5 \pm 1.1$ mM vs. $Lac_{brain}(Crtc1^{-/-}) = 1.6 \pm 0.5$ mM; $p < 0.05$, Student's t test), from the non-edited spectra quantification and the final blood lactate measurements (Lac_{blood}). An allostatic load refers to an "excess" in physiological/cellular dynamic adaption to match energetic needs in response to external stimuli [44]. To assess the level of mitochondrial allostatic pressure, the relative "oxidative allostatic loads" for *Crtc1*$^{-/-}$ mice were calculated for excitatory and inhibitory neurons separately, considering neurotransmission activity relative to mitochondrial ATP production, using following equation: Relative excitatory load $= (V_{NT}^{e}/V_{ATP(OX)}^{e})_{Crtc1^{-/-}}/(V_{NT}^{e}/V_{ATP(OX)}^{e})_{WT}$ and relative inhibitory load $= ((V_{NT}^{i} + V_{ex}^{i})/V_{ATP(OX)}^{i})_{Crtc1^{-/-}}/((V_{NT}^{i} + V_{ex}^{i})/V_{ATP(OX)}^{i})_{WT}$, where V_{NT}^{e} and $(V_{NT}^{i} + V_{ex}^{i})$ are the excitatory and inhibitory neurotransmission cycling activities respectively, and $V_{ATP(OX)}^{e}$ and $V_{ATP(OX)}^{i}$ are the excitatory and inhibitory ATP production rates from mitochondria.

Statistics

Statistics were all performed with GraphPad Prism (GraphPad Software, San Diego, CA, USA). All values are given as mean ± s.e.m. unless stated otherwise. p values of $p < 0.05$ were considered statistically significant. Metabolite data from high-resolution ^{1}H- and ^{31}P-NMR were analyzed with a non-parametric Mann–Whitney test. Longitudinal measurements (behavior and metabolites) were analyzed using two-way analysis of variance (ANOVA) with genotype and time as both factors. Gene expression and metabolic comparisons with two factors (genotype and treatment) were analyzed with two-way ANOVA and a Bonferroni post hoc test when appropriate. Data from the OSFST behavioral measurements were analyzed with a two-way ANOVA with repeated measures followed by a Fisher LSD post hoc test [31]. Standard deviation of metabolic flux estimates was obtained from 300 Monte–Carlo simulations. Flux comparisons between *Crtc1*$^{-/-}$ and WT mice were performed with a permutation analysis with 2000 random permutations, followed by individual two-tailed Student's t tests [45]. All the other comparisons between *Crtc1*$^{-/-}$ and WT animals were performed with paired or unpaired Student's t test.

RESULTS

Deletion of *Crtc1* is associated with a neuroimaging fingerprint of reduced hippocampal neuroenergetics

We first determined whether deletion of *Crtc1* in mice has measurable metabolic consequences in the brain using proton MRS (^{1}H-MRS) and MRI. Animals were scanned at an early age (6 weeks) in a 14.1 Tesla scanner (Fig. 1A) to acquire MRI whole brain anatomical images and ^{1}H-MRS spectra of DH and PFC. When comparing the neurochemical profiles of *Crtc1*$^{-/-}$ mice as compared to their WT (i.e., *Crtc1*$^{+/+}$) littermates (Fig. 1B, C), hippocampal neuroenergetic alterations were noted, including a reduced ratio of phosphocreatine relative to creatine (PCr/Cr; $p = 0.04$) and decreased level of lactate (Lac; $p = 0.02$). Subsequently, to evaluate the PCr to Cr ratio measured in vivo, high-resolution ^{1}H- and ^{31}P-NMR of hippocampal metabolite extracts (Fig. 1D–G) was performed in another group of mice to further assess the drop in PCr (Fig. 1E; $p = 0.04$). In addition, an increase in inorganic phosphate was observed (P_i; $p = 0.03$), in line with higher PCr hydrolysis, while ATP levels and the NADH/NAD$^+$ ratio were similar in both groups (Fig. 1G, n.s.). Interestingly, the neurochemical profile of PFC (Fig. S1A, B) did not indicate neuroenergetic alterations, but an increase in total choline (tCho; $p = 0.0006$), i.e., glycerophosphorylcholine (GPC) and phosphocholine (PCho), in *Crtc1*$^{-/-}$ mice. This rise in phospholipid-related metabolites coincided with bigger prefrontal volume (Fig. S1C), as measured from MRI images, suggesting potential prefrontal inflammation. These distinct observations between PFC and DH could not be attributed to differences in *Crtc1* brain regional expression, as total *Crtc1* mRNA was comparable between both regions in the WT mice (Fig. S1D). Taken together, these results indicate that *Crtc1* deletion affects hippocampal energy metabolism and prefrontal integrity, producing a measurable fingerprint using neuroimaging modalities.

Deletion of *Crtc1* impacts hippocampal glycolytic metabolism with subsequent mitochondrial allostatic load

We next aimed to identifying the origin of hippocampal metabolic alterations by assessing glycolytic and mitochondrial energetic

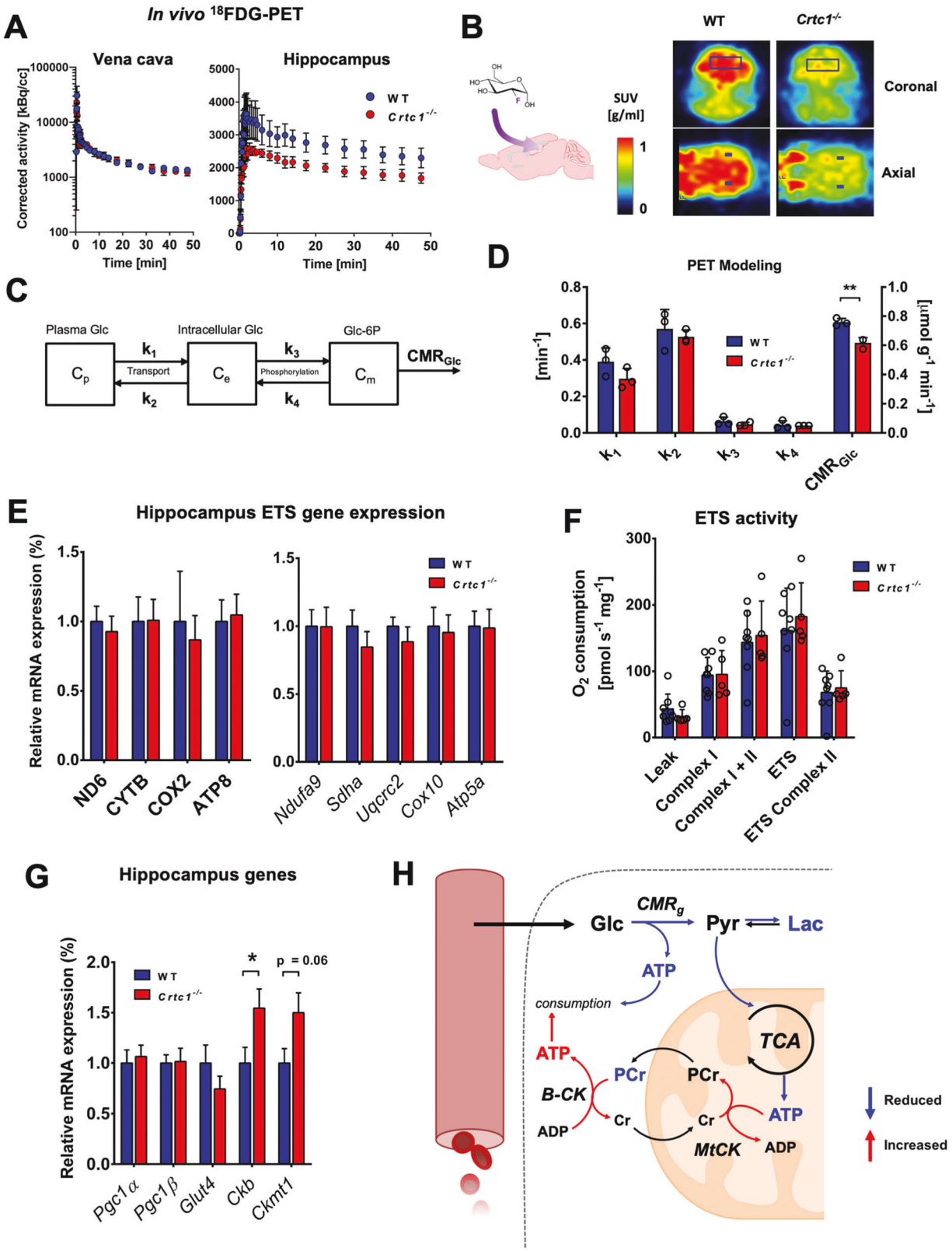

function. Measuring brain glucose utilization with PET, upon infusion of ^{18}F-fluorodeoxyglucose (^{18}FDG) radiotracer, revealed that *Crtc1*$^{-/-}$ mice have less glucose consumption in the hippocampus compared to controls (Fig. 2A–D). Accumulation curves of ^{18}F in hippocampus, resulting from cellular incorporation of ^{18}FDG into ^{18}FDG-6P through the action of hexokinase, were clearly reduced in the *Crtc1*$^{-/-}$ mice (Fig. 2A, B), which was associated with a 20% lower cerebral metabolic rate of glucose obtained by mathematical modeling (CMR_{Glc}; Fig. 2C, D; $p = 0.0045$). Interestingly, the ability to produce energy through mitochondrial function did not appear to be affected per se, as we did not observe any significant alteration of electron transport

Fig. 2 Deletion of *Crtc1* impacts hippocampal glycolytic metabolism with subsequent mitochondrial allostatic load. A–C In vivo ^{18}FDG-PET results show reduced glycolytic activity in the hippocampus of in *Crtc1*$^{-/-}$ mice compared to wild-type (WT) mice. **A** Time course of the radioactive decay-corrected activity, to the start of the acquisition, for vena cava (left) and hippocampus (right) in wild-type ($n = 3$) and *Crtc1*$^{-/-}$ ($n = 3$) mice. **B** Schematic of brain ^{18}FDG uptake (left) and heat-maps of standard uptake values (SUVs) at steady-state (last 5 min) after ^{18}FDG delivery in one *Crtc1*$^{-/-}$ and wild-type mouse (right). **C** Mathematical model used for assessing glucose entry and metabolism from PET data. Glucose (Glc) is in exchange between one plasma (C_p) and one intracellular (C_e) pool with kinetic constants k_1 and k_2. A glucose-6-phosphate (Glc-6P) pool (C_m) is produced from phosphorylation of intracellular Glc via kinetic constants k_3 and k_4. Glc-6P is then further metabolized through glycolysis, referred to here as the "cerebral metabolic rate of glucose" (CMR_{Glc}), **D** Glucose metabolism parameter estimates from mathematical modeling of hippocampal ^{18}FDG-PET data. $^{**}p < 0.005$, unpaired Student's *t* test. **E–G** Mitochondrial status is not directly affected by deletion of *Crtc1*. **E** Relative electron transfer system (ETS) gene expression in dorsal hippocampus of wild-type ($n = 9$) and *Crtc1*$^{-/-}$ ($n = 7$) mice. mtDNA-encoded: ND6, complex I; CYTB, complex II; COX2, complex IV; ATP8, complex V. nDNA-encoded: *Ndufa9*, complex I; *Sdha*, complex II; *Uqcrc2*, complex III; *Cox10*, complex IV; *Atp5a*, complex V. **F** Mitochondrial respirometry in dorsal hippocampus of wild-type ($n = 8$) and *Crtc1*$^{-/-}$ ($n = 5$) mice. **G** Mitochondrial gene expression in dorsal hippocampus of wild-type ($n = 9$) and *Crtc1*$^{-/-}$ ($n = 8$) mice. *Pgc1α* and *β*, Peroxisome proliferator-activated receptor gamma coactivator 1 alpha and beta; *Ckb*, creatine kinase B-type; *Ckmt1*, creatine kinase mitochondrial type. **H** Schematic representation of hippocampal mitochondrial allostatic load. Reduced glycolytic function leads to fewer pyruvate available for oxidation in the mitochondria. The resulting lack of ATP produced from mitochondria and glycolysis is compensated by higher PCr hydrolysis, which helps buffer ATP depletion to maintain homeostasis and potentially stimulated by the upregulation of creatine kinases expression. Glc glucose, Pyr pyruvate, B-CK cytoplasmic creatine kinase, MtCK mitochondrial creatine kinase. All data are shown as mean ± s.e.m.

system expression (mtDNA- or nDNA-encoded; Fig. 2E) or respiration efficiency (Fig. 2F) in *Crtc1*$^{-/-}$ mice. Furthermore, no apparent difference in master regulators of mitochondrial biogenesis and function, i.e., PGC1α and β (peroxisome proliferator-activated receptor gamma coactivator 1α and β), was observed (Fig. 2G), strengthening the idea that mitochondrial capacity is not directly affected by deletion of *Crtc1*. Nevertheless, the low PCr/P_i ratio described earlier strongly suggests that mitochondria are under pressure to maintain homeostasis, as supported by creatine kinase (cytoplasmic, *Ckb*; and mitochondrial, *Ckmt1*) upregulation in *Crtc1*$^{-/-}$ mice (Fig. 2G). In sum, these results suggest that the low hippocampal PCr and Lac content observed in young *Crtc1*$^{-/-}$ mice arises from impaired glycolytic metabolism, creating a pressure to maintain steady ATP levels (Fig. 2H), a situation described as an allostatic load.

Hippocampal energetic status reflects the depressive-like behavior of *Crtc1*$^{-/-}$ mice

To test the stability over time of these hippocampal energetic alterations and determine if they were associated with the depressive-like behavior of *Crtc1*$^{-/-}$ mice, we subjected WT and *Crtc1*$^{-/-}$ animals to social isolation from the age of 6 weeks and monitored their neurochemical profile and behavior longitudinally (Fig. 3A). Social isolation was used to ensure a comparable social environment between groups and reduce aggression-related effects within cages [30]. A higher level of depressive-like behavior was observed (Fig. 3B) for *Crtc1*$^{-/-}$ mice under basal conditions (6 weeks of age) as reflected in forced swim test (FST; $p = 0.02$) but not in tail suspension test (TST; n.s). Surprisingly, 18 weeks of our social isolation protocol had an opposite effect on the behavior of the two groups (averaged *z*-scores, Interaction: $F_{2,28} = 10.26$, $p = 0.0005$; TST, Interaction: $F_{2,28} = 5.16$, $p = 0.012$; FST, Interaction: $F_{2,28} = 3.87$, $p = 0.035$; two-way ANOVA). Moreover, an inversion in the hippocampal energetic profile (Fig. 3C) coincided with this switch in behavior (Lac, Interaction: $F_{2,28} = 7.32$, $p = 0.003$; PCr, Interaction: $F_{2,28} = 4.78$, $p = 0.017$; PCr/Cr, Interaction: $F_{2,28} = 2.79$, $p = 0.08$; two-way ANOVA). Interestingly, hippocampal glucose concentration rose only in *Crtc1*$^{-/-}$ mice upon social isolation (Time effect: $F_{2,28} = 3.43$, $p = 0.050$, two-way ANOVA; *Crtc1*$^{-/-}$ 6-weeks vs. 6-months, $^{*}p < 0.05$, Bonferroni's test). We then performed correlational analyses to further relate metabolite hippocampal markers with behavior (Fig. 3D) and found a significant negative correlation between the depressive-like behavior and Lac (Lac vs. averaged *z*-scores: $R = -0.35$, $p = 0.01$). To test whether these metabolic modifications were associated with a change in gene expression, we analyzed relative mRNA content in DH at the end of the protocol (Fig. 3E and Fig. S2A) and found a difference in *Pgc1α* ($p = 0.04$) and *Glut4* ($p = 0.01$) between the two groups, while creatine kinases levels were no longer significantly different (n.s.). Notably, differences in depressive-like behavior between *Crtc1*$^{-/-}$ and WT mice were not related to locomotor activity at any age (Fig. S2B, n.s.) or PFC volume and tCho content, which both correlated with each other and remained increased in *Crtc1*$^{-/-}$ independently of the animal's age (Figs. S2C and S3; tCho, Genotype effect: $F_{1,148} = 12.89$, $p = 0.003$; Volume, Genotype effect: $F_{1,42} = 14.61$, $p = 0.0004$; two-way ANOVA; Correlation: $R = 0.31$, $p = 0.03$). Importantly, our social isolation protocol stimulated the development of a MeS-related phenotype in both groups as suggested by the rise in body weight (Fig. 3F), which developed faster over time for *Crtc1*$^{-/-}$ mice (Genotype effect: $F_{1,14} = 5.84$, $p = 0.01$; Interaction: $F_{2,28} = 5.11$, $p = 0.03$, two-way ANOVA), and the high level of blood MeS markers (insulin, glucose and triglycerides), which were not significantly different between the groups (Fig. 3G; n.s.). Overall, these results confirm that the hippocampal neuroenergetic status of *Crtc1*$^{-/-}$ mice reflects their depressive-like behavior and indicate an apparent dependence on the experienced environment.

Restoring hippocampal energy balance with energy-boosting ebselen mood-stabilizer rescues depressive-like behavior in *Crtc1*$^{-/-}$ mice

Social isolation appeared to be beneficial for *Crtc1*$^{-/-}$ mice, consistent with their known aggressive behavior and social impairments toward other individuals [30]. We thus hypothesized that a repeated open-space forced swim test (OSFST) protocol (Fig. 4A), which contains an environmental- rather than social-stress component, would challenge neuroenergetics in both groups of mice. In parallel, we tested whether improving brain metabolism with an energy-stimulating compound would reverse the stressful effects of the OSFST. To maximize the translational relevance of our findings, we decided to treat animals by oral administration of ebselen, a neuroprotective and antioxidant compound [46] with comparable pharmacological properties as lithium (e.g., inhibitor of GSK3β and inositol monophosphatase) [47] and with a strong clinical potential [48, 49]. After 4-consecutive days of swimming sessions and establishment of a stable depressive-like behavior in all groups of mice, animals were treated with either ebselen or vehicle twice a day for 3 weeks. As expected, the depressive-like behavior, measured as immobility time in OSFST, was higher in *Crtc1*$^{-/-}$ mice over time (Fig. 4B; Genotype effect: $F_{1,10} = 65.09$, $p < 0.0001$, two-way ANOVA). Ebselen rescued the behavior of *Crtc1*$^{-/-}$ mice (Interaction: $F_{1,10} = 41.84$, $p < 0.0001$; Treatment effect: $F_{1,10} = 5.45$, $p = 0.04$, two-way ANOVA) and led to an improvement in hippocampal energy metabolism (Fig. 4C, D). More specifically,

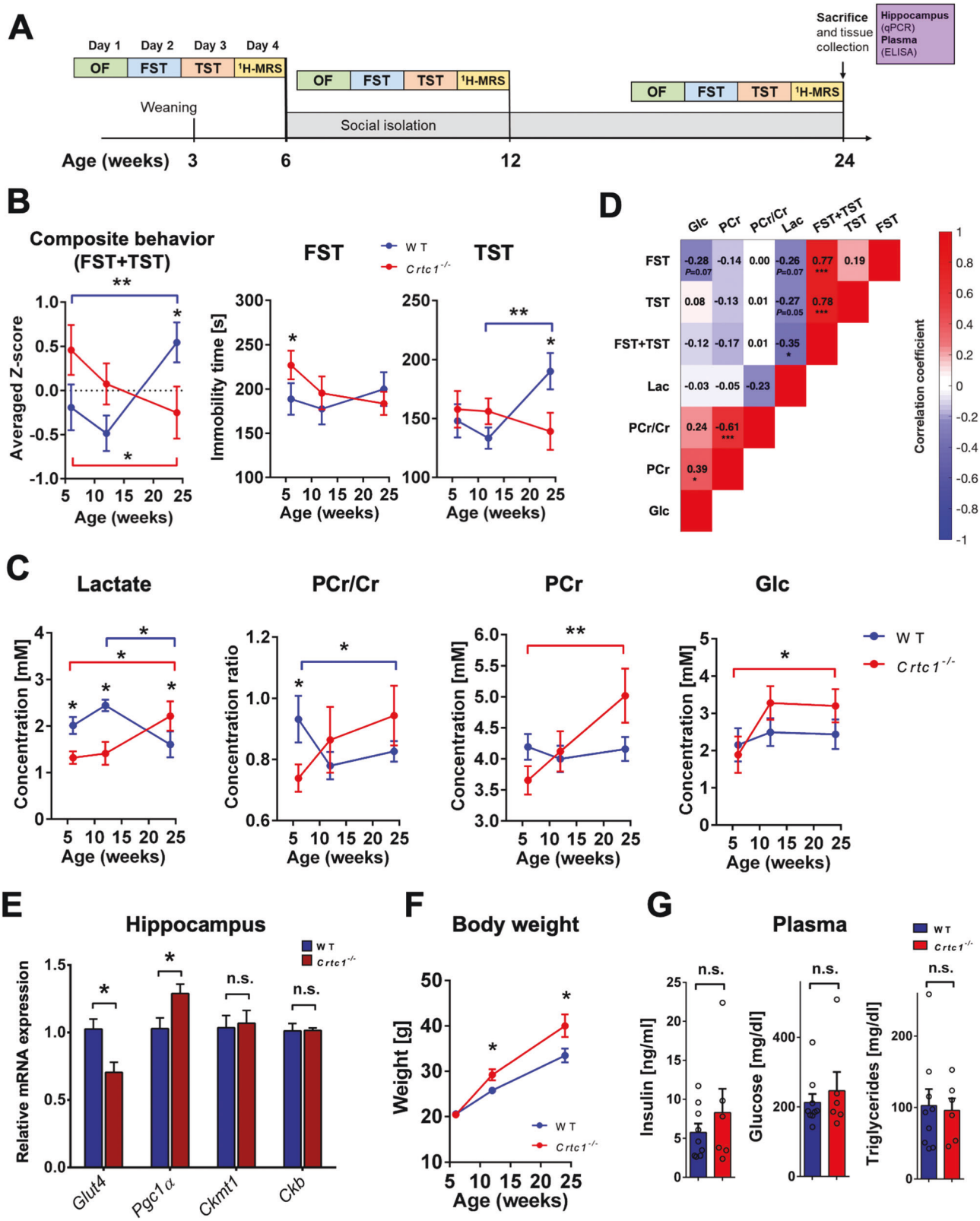

ebselen raised hippocampal PCr content (Fig. 4D; ΔPCr/Cr, Treatment effect: $F_{1,31} = 4.41$, $p = 0.04$; two-way ANOVA) compared to the untreated groups, but lowered lactate levels in *Crtc1*$^{-/-}$ mice at the end of the study protocol (Fig. 4C; Lac day 21, $p = 0.045$; unpaired *t*-test), in line with enhanced mitochondrial activity. Furthermore, the difference in energy metabolite content correlated with a difference in behavior (ΔPCr/Cr, $R = -0.42$, $p = 0.02$; ΔLac, $R = 0.41$, $p = 0.01$) suggesting that both events were linked (Fig. 4E). Gene expression analysis (Fig. 4F and Fig. S4A) supports that ebselen stimulated DH mitochondrial function, as highlighted by a treatment

Fig. 3 Hippocampal neuroenergetic status reflects the depressive-like behavior of *Crtc1*$^{-/-}$ mice. A Experimental design, and timeline of the longitudinal protocol used involving social isolation. Wild-type (WT; $n = 10$) and *Crtc1*$^{-/-}$ ($n = 6$) mice underwent a set of behavioral tests including an open-field test (OF; day 1), a forced swim test (FST; day 2) and a tail-suspension test (TST; day 3) followed by a ^{1}H-MRS scan on day 4. After this first set of experiments, animals were isolated at the age of 6 weeks and the whole procedure was repeated at 12 and 24 weeks of age. After the last ^{1}H-MRS scan, animals were sacrificed, and hippocampal and plasma samples were collected for analysis. **B** A switch in depressive-like behavior between *Crtc1*$^{-/-}$ and wild-type mice occurs after 18 weeks of social isolation as revealed by the inversion in immobility time in TST (right panel; Interaction: $F_{2,28} = 5.16$, $p = 0.012$), FST (center panel; Interaction: $F_{2,28} = 3.87$, $p = 0.035$) and averaged *z*-score of TST and FST (left panel; Interaction: $F_{2,28} = 10.26$, $p = 0.0005$). Two-way ANOVA, followed by Fisher LSD post hoc test; $^{*}p < 0.05$, $^{**}p < 0.01$. **C** Hippocampal neuroenergetic profile switches between *Crtc1*$^{-/-}$ and wild-type mice at the end of 18 weeks of isolation as revealed by the inversion of lactate concentration (left panel; Interaction: $F_{2,28} = 7.32$, $p = 0.003$), PCr/Cr ratio (center left panel; Interaction: $F_{2,28} = 2.79$, $p = 0.08$) and PCr (center right panel; Interaction: $F_{2,28} = 4.78$, $p = 0.017$). Hippocampal glucose levels increased in the *Crtc1*$^{-/-}$ group only at the end of the 18 weeks of isolation (Time effect: $F_{2,28} = 3.43$, $p = 0.050$). Two-way ANOVA, followed by Bonferroni's post hoc test; $^{*}p < 0.05$, $^{**}p < 0.01$. **D** Correlative analysis between depressive-like behavior and hippocampal energy metabolite content. A significant negative correlation between Lac and behavior was found when results from FST and TST were considered together ($R = -0.351$, $p = 0.013$). Color code represents Pearson's correlation coefficient and the analysis included all longitudinal age time points. Pearson's *R*s are shown for each correlation with associated *p* value (uncorrected for multiple comparisons); $^{*}p < 0.05$, $^{***}p < 0.0001$. **E** At the end of 18 weeks of isolation, hippocampal levels of *Pgc1a* mRNA were higher while *Glut4* levels were lower in *Crtc1*$^{-/-}$ as compared to wild-type mice. Mitochondrial and cytoplasmic creatine kinases were not significantly different (n.s.) between the two groups. Unpaired Student's *t* test, $^{*}p < 0.05$. **F** Body weight of all animals increased significantly over time (Time effect: $F_{2,28} = 123.2$, $p < 0.0001$) but increased more in the *Crtc1*$^{-/-}$ group (Genotype effect: $F_{1,14} = 5.84$, $p = 0.030$; Interaction: $F_{2,28} = 5.11$, $p = 0.013$). Two-way ANOVA followed by Fisher LSD post hoc test $^{*}p < 0.05$. **G** Plasma markers of metabolic syndrome (insulin, glucose and triglycerides) were high in both groups but not significantly different from each other (n.s.).

effect observed in *Pgc1a* ($F_{1,27} = 13.28$, $p = 0.009$), *Glut4* ($F_{1,27} = 8.22$, $p = 0.001$) and *Ckmt1* ($F_{1,27} = 4.79$, $p = 0.04$, two-way ANOVA) mRNA content. Interestingly, treatment did not affect *Ckb* expression, which was slightly increased in the *Crtc1*$^{-/-}$ group (Genotype, $F_{1,27} = 3.79$, $p = 0.06$, two-way ANOVA) echoing our results in basal condition. Of note, Western blot analysis of creatine kinases revealed an overall effect on protein levels predominantly carried by the mitochondrial-type enzyme which was increased by ~60% in the *Crtc1*$^{-/-}$ group as compared to WT (Fig. S4B; U-MtCK: Genotype effect: $F_{1,23} = 25.06$, $p < 0.0001$). To test for direct involvement of CRTC1 in the transcriptional regulation of our genes of interest, we assessed CRTC1-gene interactions in the hippocampus of 8-week-old male mice using a small-scale chromatin immunoprecipitation sequencing (ChIP-seq) approach (ChIP-seq antibody validation service, Active Motif, Inc., Carlsbad, CA, USA). This experiment allowed us to validate two CRTC1 antibodies and to determine the presence or absence of CRTC1's binding for up to 8 genes of interest. These preliminary results suggested that both *Ckb* and *Ckmt1* are under the direct regulatory control of CRTC1 (data not shown). Importantly, ebselen did not interfere with the increased body weight and high insulin and triglyceride levels in *Crtc1*$^{-/-}$ mice (Fig. 4G; Treatment effect, n.s), confirming a brain-specific mechanism, neither did ebselen affect PFC volume and tCho concentration differences observed in *Crtc1*$^{-/-}$ mice (Fig. S4C–E). Finally, to assess the potential clinical relevance of the identified neuroimaging markers we determined their specificities and sensitivities using ROC curves (Fig. S4F, G). Prefrontal volume and tCho concentration were able to differentiate *Crtc1*$^{-/-}$ mice from their WT counterparts with an area under the curve (AUC) of up to 82% (95% CI 0.755–0.886), when combined into an averaged *z*-score. The ability of hippocampal neuroenergetic markers to differentiate mice with "high" levels of depressive-like behavior from those with "low" levels was more modest, with an AUC of up to 66% (95% CI 0.555–0.756), when combined into an averaged *z*-score. In summary, stimulating mitochondrial energy metabolism was able to rescue the depressive-like behavior induced by stress in *Crtc1*$^{-/-}$ mice, leading to neuroimaging-based modifications that followed the treatment response.

GABAergic dysfunction links impaired hippocampal glucose metabolism with depressive-like behavior in *Crtc1*$^{-/-}$ susceptible mice

Finally, to assess the relative brain cellular metabolic contributions, we acquired indirect ^{13}C-carbon magnetic resonance spectroscopy (^{1}H-[^{13}C]-MRS; Fig. 5A) data to assess metabolic fluxes using mathematical modeling. Fractional isotopic ^{13}C-enrichment (FE) of brain glucose and downstream metabolites revealed clear group differences in animals of 6 weeks in age (Fig. 5B) involving metabolites associated with glycolysis (U-Glc, LacC3), tricarboxylic acid (TCA) cycle (GluC4) and GABAergic neurons metabolism (GABAC2-4). When fitting the mathematical models to the ^{13}C-labeling data (Fig. 5C and Fig. S5A), we found that reduced glucose consumption (i.e., CMR_{Glc}) led to a drop of TCA cycle activity in both excitatory (−36%, $p < 0.0001$) and inhibitory (−14%, $p = 0.01$) neurons of *Crtc1*$^{-/-}$ mice. Neurotransmission flux was overall increased (Fig. S5B; $V_{NT} = 0.06 \pm 0.01$ for WT vs. 0.09 ± 0.02 µmol/g/min for *Crtc1*$^{-/-}$, $p = 0.004$) when considering metabolism as a whole (1-compartment) but analysis with a more complex model (pseudo 3-compartment model, i.e., that considers the relative excitatory and inhibitor metabolic contributions and assuming similar glial metabolism) indicated this effect was more pronounced in GABAergic ($V_{NT}^{i} + V_{ex}^{i}$; 6-fold increase) than glutamatergic (V_{NT}^{e}; 2-fold increase) neurotransmission. Importantly, the increase in GABA labeling (Fig. 6B) did not arise from an increase in GAD activity according to our model ($V_{GAD} = 0.32 \pm 0.06$ for WT vs. 0.30 ± 0.08 µmol/g/min for *Crtc1*$^{-/-}$, n.s.) but reflected a dilution originating from exchange between two GABA pools and possibly triggered by GABAergic neurotransmission recycling (Fig. S5C; $V_{ex}^{i} = 0.0006 \pm 0.0002$ for WT vs. 0.007 ± 0.003 µmol/g/min for *Crtc1*$^{-/-}$, $p = 0.02$), in line with a probable inhibitory neuron hyperactivity. Furthermore, despite the relatively higher drop of ATP production rate in excitatory (−35%) compared to inhibitory (−15%) neurons (Fig. S5D), the relative oxidative allostatic load calculated as the neurotransmission relative to ATP production (see methods) indicated a ~2.7-fold higher load for inhibitory neurons (8.4x higher in *Crtc1*$^{-/-}$ mice) relative to excitatory neurons (3.1x higher in *Crtc1*$^{-/-}$ mice), suggesting that GABAergic inhibitory neurons might be more at risk.

To further determine if the GABAergic system is particularly impacted by hippocampal energetic impairments, we re-analyzed main GABAergic gene expression in our different experimental protocols. Interestingly, levels of *Gad2* and parvalbumin (*Pvalb*) were strongly associated with the behavioral state of the animals (Fig. 5D–F). At the age of 6 weeks, *Gad2* was lower in *Crtc1*$^{-/-}$ mice ($p = 0.04$) when depressive-like behavior was high (Fig. 3B), while it was increased after social isolation ($p = 0.03$; Fig. 5D) when the behavior was inverted as well (Fig. 3B). Importantly, ebselen restored the levels of both *Gad2* (Interaction: $F_{1,27} = 5.53$, $p = 0.03$) and *Pvalb* (treatment effect: $F_{1,24} = 4.28$, $p = 0.049$) in *Crtc1*$^{-/-}$ mice after OSFST. Finally, *Pvalb* was the only gene that correlated directly

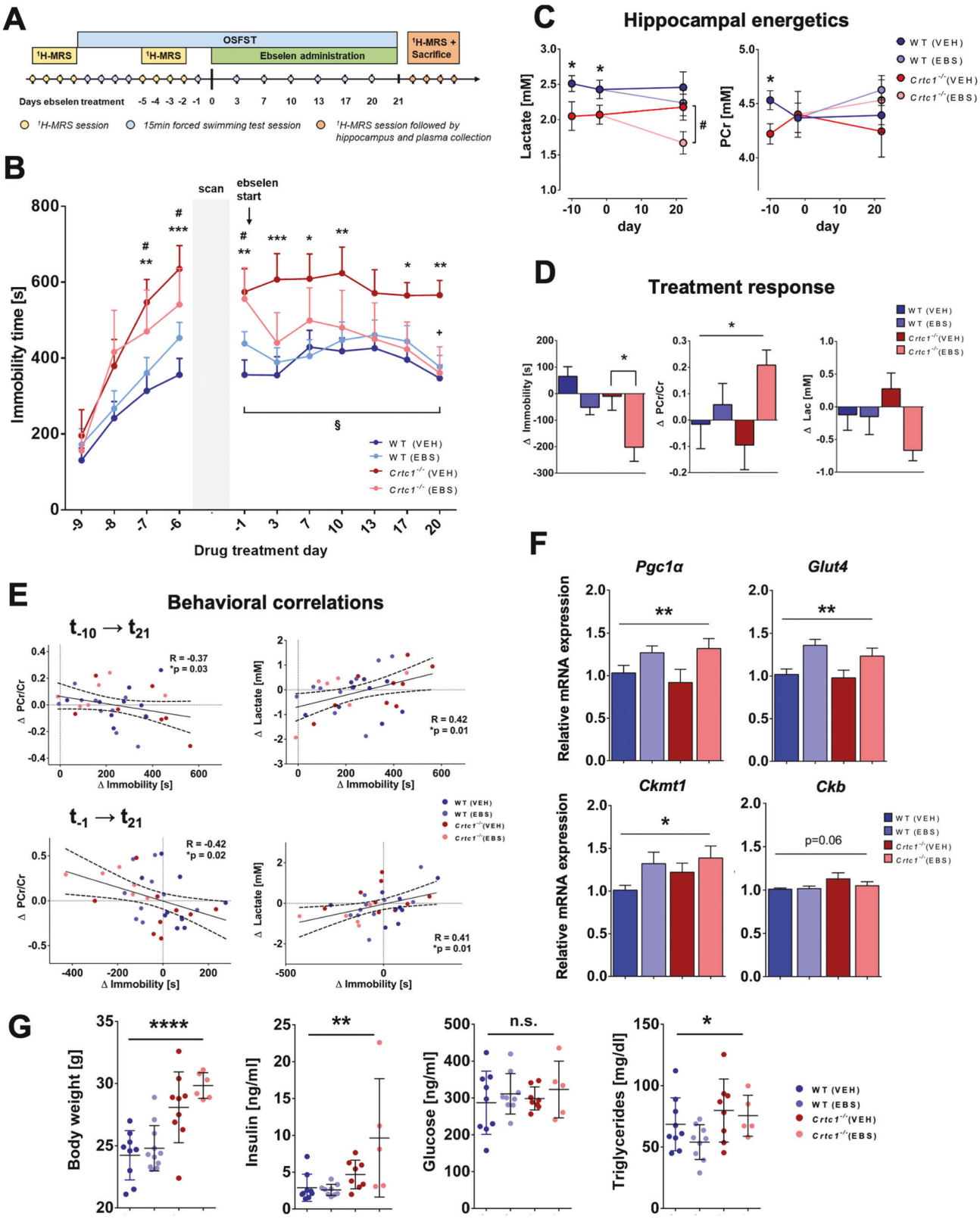

with the level of depressive-like behavior in both experiments (Social isolation: $R = -0.55$, $p = 0.03$; OSFST + treatment: $R = -0.69$, $p = 0.0001$). The above results suggest that the hippocampal GABAergic system might be mechanistically involved in the depressive-like behavior induced by neuroenergetic impairments.

DISCUSSION

Understanding how genetic and environmental factors interact in metabolic diseases and how they impact normal brain and behavior is central for better diagnosing and treating related MD. Because of its central role in regulating brain metabolism and its

Fig. 4 Restoring hippocampal energy balance with energy-boosting ebselen mood stabilizer rescues depressive-like behavior in *Crtc1*$^{-/-}$ mice. A Experimental design, and timeline of the ebselen treatment protocol during open-space forced swim test (OSFST). First, animals underwent a single basal ^{1}H-MRS scan (during days −13 to −10), followed by 4 consecutive forced swimming sessions (day −9 to −6). During days −5 to −2, animals underwent a second ^{1}H-MRS scan and a fifth swimming session on day −1, prior to the treatment start. Animals were administered ebselen (wild-type(EBS), $n = 8$; *Crtc1*$^{-/-}$(EBS), $n = 6$) or vehicle (wild-type(VEH), $n = 9$; *Crtc1*$^{-/-}$(VEH), $n = 9$) twice daily from day 0 and until the end of the OSFST protocol (day 21), while swimming sessions were repeated regularly every 3–4 days. A final ^{1}H-MRS scan was performed at the end of the study (between days 22–25), with subsequent hippocampal and plasma collection for analyses. **B** Depressive-like behavior in the OSFST was higher in the *Crtc1*$^{-/-}$ mice (Genotype effect: $F_{1,10} = 65.09$, $p < 0.0001$) but reduced by ebselen (Treatment effect: $F_{1,10} = 5.45$, $p = 0.04$, interaction: $F_{1,10} = 41.84$, $p < 0.0001$). Immobility of all *Crtc1*$^{-/-}$ mice was increased after the first 4 days swimming session (**$p < 0.01$, ***$p < 0.005$ for VEH and $^{\#}p < 0.05$ for EBS vs. their respective wild-type group). Depressive-like behavior of *Crtc1*$^{-/-}$ VEH group remained significantly higher than wild-type over the 21 days of test (*$p < 0.05$, **$p < 0.01$ and ***$p < 0.005$ for VEH *Crtc1*$^{-/-}$ vs. VEH wild-type). After the 21 days of OSFST, the depressive-like behavior of the treated *Crtc1*$^{-/-}$ animals was significantly reduced ($^{+}p < 0.05$ compared to *Crtc1*$^{-/-}$ VEH at day 20 and $^{\S}p < 0.05$ compared to *Crtc1*$^{-/-}$ EBS at day 0). Two-way ANOVA for repeated measures, followed by Fisher LSD post hoc test. **C** Hippocampal energy metabolite concentrations during the OSFST protocol. Lactate and PCr content were lower in *Crtc1*$^{-/-}$ animals relative to wild-type animals under basal conditions (days −13 to −10; Unpaired Student's *t* test, *$p < 0.05$; wild-type, $n = 22$; *Crtc1*$^{-/-}$, $n = 16$), but only lactate remained lower in *Crtc1*$^{-/-}$ animals after ebselen treatment (days 22–25; Unpaired Student's *t* test, $^{\#}p < 0.05$; wild-type(EBS), $n = 8$; *Crtc1*$^{-/-}$(EBS), $n = 6$). **D** Ebselen treatment reduced depressive-like behavior and increased hippocampal high-energy phosphate content (difference between day 21 and day 0). Ebselen treatment increased the PCr/Cr ratio (Treatment effect: $F_{1,31} = 4.41$, *$p = 0.044$, two-way ANOVA) and tended to reduce lactate (Treatment effect: $F_{1,31} = 3.49$, $p = 0.071$, two-way ANOVA), together with immobility reduction (Treatment effect: $F_{1,31} = 13.7$, $p = 0.0008$; Genotype effect: $F_{1,31} = 7.30$, $p = 0.011$; two-way ANOVA, followed by Bonferroni's test, *$p < 0.05$). **E** (top) The increase in immobility from baseline (day −10) as a result of OSFST (day 21) correlated with a reduction in PCr/Cr ($R = -0.37$, *$p = 0.03$) and rise in lactate ($R = 0.42$, *$p = 0.01$). (bottom) Immobility reduction (from day −1) as a result of treatment (day 21) correlated with a rise in PCr/Cr ($R = -0.42$, *$p = 0.02$) and a drop of lactate ($R = 0.41$, *$p = 0.01$). **F** Ebselen induced expression of energy-related genes in hippocampus. Treated animals had higher mRNA level of *Pgc1α* (Treatment effect: $F_{1,27} = 13.28$, **$p = 0.0087$), *Glut4* ($F_{1,27} = 8.22$, **$p = 0.0011$) and *Ckmt1* ($F_{1,27} = 4.79$, *$p = 0.037$). Relative cytoplasmic creatine kinase (*Ckb*) expression tend to increase in *Crtc1*$^{-/-}$ mice at the end of the OSFST protocol (Genotype effect: *Ckb*: $F_{1,27} = 3.78$, $p = 0.06$; *Ckmt1*: $F_{1,27} = 1.59$, $p = 0.21$). Two-way ANOVA. **G** *Crtc1*$^{-/-}$ showed significantly higher body weight (Genotype effect: $F_{1,31} = 37.7$, ****$p < 0.0001$), plasma insulin ($F_{1,27} = 12.24$, **$p < 0.0016$) and triglyceride levels ($F_{1,27} = 4.78$, *$p = 0.038$) at the end of the OSFST protocol, with not treatment effect (n.s.). Two-way ANOVA; n.s. not significant. Data are reported as mean ± s.e.m.

strong association with features of MeS in psychiatric patients [11–14], *Crtc1* is a key candidate gene to understand how (neuro-) metabolic alterations can affect normal behavior. In this study, we have been able to identify reduced hippocampal energy metabolism in *Crtc1*-deficient mice that translated into measurable in vivo neuroimaging markers. We have demonstrated that these neurochemical impairments were associated with animal depressive-like behavior, which could be reversed with an energy-boosting treatment known for its mood-stabilizing properties. Finally, we provide evidence for a hyper-activation and allostatic load of the hippocampal GABAergic system that could mediate behavioral consequences of the observed neuroenergetic imbalance.

Even though *Crtc1* is predominantly expressed in the brain [30, 50] deleting this gene in mice induces a systemic metabolic deregulation [22], such as insulin resistance and obesity, together with a depressive-like phenotype [30, 31]. As male *Crtc1*$^{-/-}$ mice show a stronger depressive-like phenotype with a more severe comorbid obesity than females [21, 23, 29], we decided to capitalize on the former to focus on mechanistic aspects rather than sex differences in our neuroimaging study. While the association of MeS and behavioral alterations is likely to be complex and multifactorial, we report a clear link between brain glucose uptake and depressive-like behavior. Specifically, low glycolytic activity in *Crtc1*$^{-/-}$ mice was associated with reduced levels of lactate and increase in high-energy phosphate hydrolysis (i.e., high level of P_i and low levels of PCr) in hippocampus that correlated well with animal behavior (Fig. 1). This imbalance in PCr/Cr level appeared to be driven by changes in creatine kinases expression, which might be directly regulated by CRTC1, as suggested by our ChIP-seq preliminary data. Importantly, our results indicate reduced hippocampal glucose uptake capacity rather than lower demand, as the neuronal activity relative to energy production (V_{NT}/V_{TCA}) was found to be ~3-fold higher for the *Crtc1*$^{-/-}$ mice (Fig. 5A–C and Fig. S5), pointing toward a difficulty in matching energy production with neuronal needs, or what is defined as an allostatic load [44]. This fits well with the idea that CRTC1 is required for adapting energy homeostasis according to neuronal requirements [22, 51] and is in line with several studies demonstrating the central role of brain energy metabolism in the resilience mechanisms against depressive-like behavior [52–56]. Of note, our results indicate that both glycolytic and mitochondrial pathways are fundamental for brain metabolic resilience and behavior rather than one route preferentially, as CMR_{Glc} deficiency in *Crtc1*$^{-/-}$ mice could be compensated by an increase in oxidative metabolism.

Considering that glucose entry in the brain is regulated by factors such as the insulin or IGF-1 receptors, known to influence mouse depressive-like behavior [57], we hypothesize that reduced hippocampal glucose uptake arises from the known insulin resistance phenotype of *Crtc1*$^{-/-}$ mice [22]. While future research will determine the exact molecular mechanisms relating *Crtc1* with brain energy capacity, our experimental data point toward the Akt/GSK3β pathway as a potential player in this process. In fact, treatment with ebselen, known to inhibit GSK3β, improved DH energetic status and behavior through enhanced hippocampal *Pgc1α* and *Glut4* expression, with only little effect on peripheral energy markers (Fig. 4G). PGC1α, as a master mitochondrial biogenesis regulator, can be inhibited through phosphorylation by GSK3β [58], possibly impacting *Glut4* expression over the MEF2C transcription factor [59]. PGC1α has been linked with depression [60] and bipolar disorders [61], and its target, PPARγ, provides a plausible link between MeS and behavior. For instance, PPARγ agonists, which are well known insulin sensitizing agents [9], show anti-depressant properties in animal models [62] and patients [63, 64] leading to improved glucose metabolism [65]. Although studies focusing on muscle cells showed that *Crtc2*, a peripheral homolog of *Crtc1*, can induce *Pgc1α* expression [66], we did not observe reduced *Pgc1α* levels as a result of *Crtc1* deletion (Figs. 2F, 3E and 4F). Nevertheless, enhancing *Pgc1α* expression restored energy metabolism and behavior in *Crtc1*$^{-/-}$ mice (Fig. 4F), suggesting that CRTC1 deficiency can be compensated through different, though converging, pathways. Of note, elevated mRNA levels of *Pgc1α*, but not *Glut4*, were associated with improved neuroenergetic profile at the end of the longitudinal study (Fig. 3E), suggesting

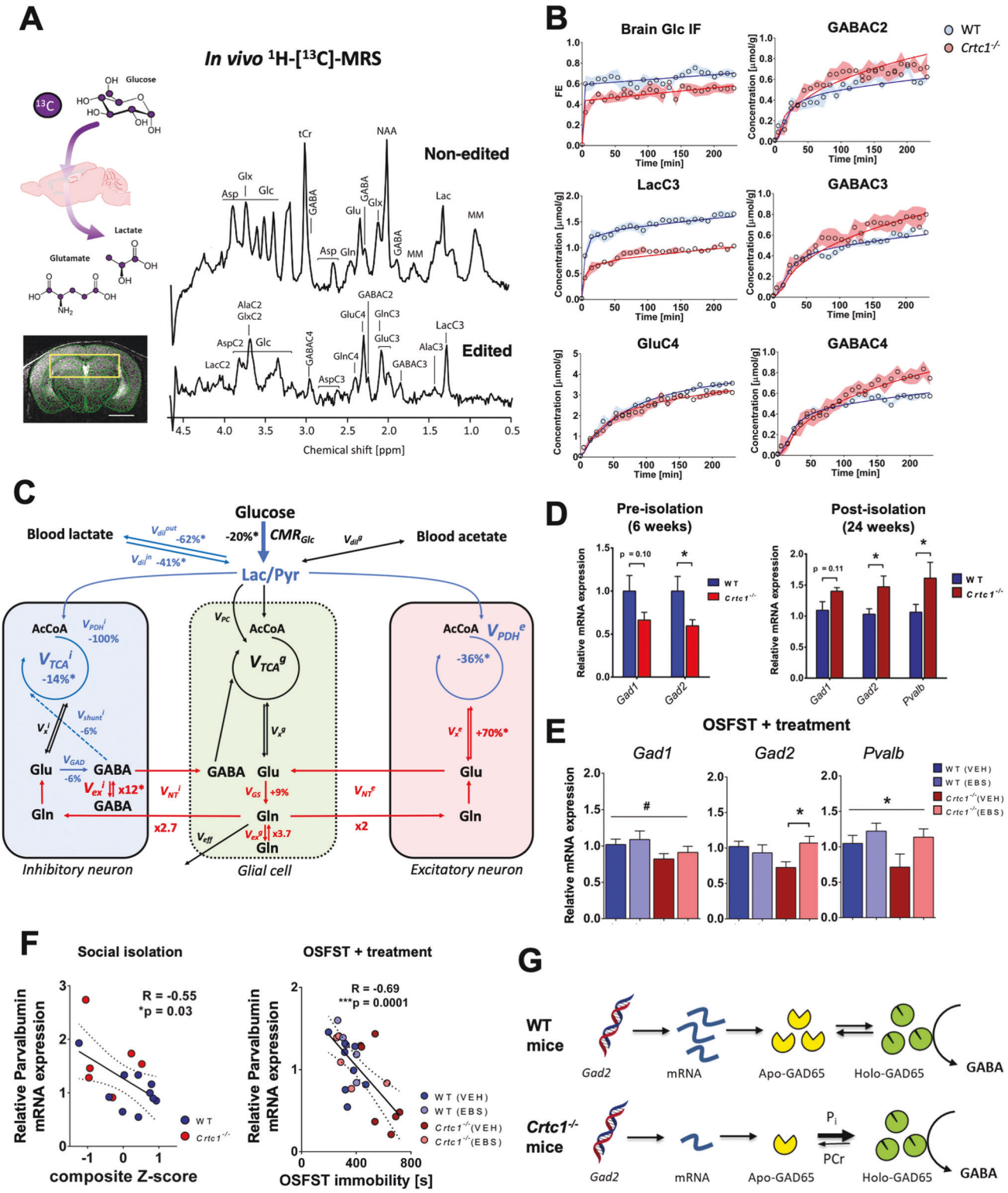

that simultaneous expression might not be required to improve behavior. Finally, despite the likely complex and multifactorial interplay of neuroenergetic genes, our results highlight a possible transcriptional control of CRTC1 on both *Ckb* and *Ckmt1*, confirming its direct mechanistic involvement in hippocampal metabolic regulation.

How then did the enhanced hippocampal energetic capacity, illustrated by higher *Pgc1a* and *Glut4* expression (Fig. 4F), not affect the behavior of WT mice, as would be expected from this model? It is plausible that efficient energy metabolism is necessary for resilience to depressive-like behavior but is not sufficient to modulate it. Energy metabolism, either mitochondrial or glycolytic, has been widely implicated in the pathophysiological mechanisms leading to depressive-like behavior in preclinical models [52, 54–56, 67] and in clinical studies [68–71]. Nevertheless, it remains unclear how altered brain energy production rates could

Fig. 5 GABAergic dysfunction links impaired hippocampal glucose metabolism with depressive-like behavior in *Crtc1*$^{-/-}$ susceptible mice. A Schematic of ^{13}C-labeled glucose brain uptake and subsequent metabolite labeling (upper left) ^{1}H-[^{13}C]-MRS spectra acquired in the bilateral dorsal hippocampus of a 6 weeks old WT mouse (right) as shown with the selected VOI (yellow box) on the associated MRI image (lower left). The non-edited spectrum (top) shows the total metabolic profile, while the edited spectrum (bottom) identifies the fraction of metabolites that have incorporated ^{13}C-labeling. Scale bar = 2 mm. **B** Fractional isotopic ^{13}C-enrichment (FE) of glucose and key metabolites in the hippocampus during ^{1}H-[^{13}C]-MRS experiment. Fitting of the data with a pseudo 3-compartment model of brain glucose metabolism is shown with a straight line for wild-type (WT; in blue) and *Crtc1*$^{-/-}$ (in red) mice. 6 weeks old wild-type ($n = 8$) and *Crtc1*$^{-/-}$($n = 8$). Data presented as mean ± s.d. **C** Schematic representation of hippocampal glucose utilization differences between wild-type and *Crtc1*$^{-/-}$ mice after metabolic flux analysis using a pseudo 3-compartment model. Metabolic fluxes that were higher in *Crtc1*$^{-/-}$ animals (compared to their wild-type littermates) are shown in red, while those found lower are shown in blue and those found without any difference or fixed during the modeling remain in black. Cerebral metabolic rate of glucose (CMR_{Glc}); brain lactate influx (V_{dil}^{in}) and outflux (V_{dil}^{out}) from blood; pyruvate dilution flux (V_{dil}^{g}); excitatory neuron TCA cycle (V_{PDH}^{e}); inhibitory neuron pyruvate dehydrogenase activity (V_{PDH}^{i}); GABA shunt flux (V_{shunt}^{i}); inhibitory neuron TCA cycle ($V_{TCA}^{i} = V_{PDH}^{i} + V_{shunt}^{i}$); glial pyruvate carboxylase (V_{PC}); glial TCA cycle (V_{TCA}^{g}); excitatory neuron (V_x^{e}), inhibitory neuron (V_x^{i}) and glial (V_x^{g}) transmitochondrial fluxes; excitatory neurotransmission flux (V_{NT}^{e}); inhibitory neurotransmission flux (V_{NT}^{i}); glutamate decarboxylase activity (V_{GAD}); Gln exchange flux (V_{ex}^{g}); GABAergic exchange flux (V_{ex}^{i}); glutamine synthetase activity (V_{GS}) and Gln efflux (V_{eff}). Relative flux increase/decrease is indicated for *Crtc1*$^{-/-}$ mice compared to WT littermates, as calculated from fluxes in µmol/g/min from Fig. S5C; and an asterisk (*) indicates a statistically significant difference between the two groups. **D** GABAergic gene expression (*Gad1*, *Gad2* and parvalbumin (*Pvalb*)) in the hippocampus under basal conditions (6 weeks age; left) or after social isolation (24 weeks age; right). Unpaired Student's *t* test, $*p < 0.05$; basal, wild-type ($n = 6$) and *Crtc1*$^{-/-}$ ($n = 6$); longitudinal, wild-type ($n = 10$) and *Crtc1*$^{-/-}$ ($n = 6$). **E** Hippocampal gene expression of *Gad1*, *Gad2* and *Pvalb* after the OSFST protocol (wild-type(VEH), $n = 9$; wild-type(EBS), $n = 8$; *Crtc1*$^{-/-}$(VEH), $n = 9$; *Crtc1*$^{-/-}$(EBS), $n = 6$). *Gad1* was significantly reduced in the *Crtc1*$^{-/-}$ group (Genotype effect: $F_{1,28} = 4.39$, $*p = 0.045$, two-way ANOVA), while ebselen treatment increased the levels of *Gad2* (Interaction: $F_{1,27} = 5.53$, $*p = 0.026$, two-way ANOVA; $*p < 0.05$, Bonferroni's post hoc test) and parvalbumin (Treatment effect: $F_{1,24} = 4.28$, $*p = 0.049$, two-way ANOVA). **F** Correlation between depressive-like behavior and level of *Pvalb* expression in the hippocampus after social isolation (left; 24 weeks of age; $R = -0.55$, $p = 0.03$) and OSFST protocols (right; 10 weeks of age; $R = -0.69$, $p = 0.0001$). The dotted lines represent the 95% confidence interval of the linear regression line. **G** Scheme of potential relation between GAD expression level, energy metabolite binding and enzyme activity.

translate into behavioral dysfunction. While several processes have been brought forward, such as metabotropic-, neuroendocrine-, inflammatory-, transcriptional-, or other responses [72–74], our results highlight the hippocampal GABAergic neurotransmitter system as a new key player in the process linking cellular allostatic load with affected neuronal output. In fact, our metabolic flux and GABAergic gene expression analyses indicate that the inhibitory system is particularly affected by low energy status and could relate to depressive-like behavior more tightly than the level of metabolism-enhancing genes or high-energy phosphates. We have previously reported that inhibitory neurotransmission in the hippocampus has high mitochondrial oxidative dependence compared to excitatory neurotransmission in mice [39]. Accordingly, here we found that low energy production capacity in *Crtc1*$^{-/-}$ mice was associated with a ~6-fold increase in hippocampal GABAergic neurotransmission cycling (Fig. 5A–C), leading to an overall higher (~2.6-fold) oxidative allostatic load in inhibitory compared to excitatory neurons. Others have shown that GABA neuronal metabolism is highly controlled by the cellular energetic status, through the action of both GAD isoforms (GAD65 and GAD67), switching from an Apo (inactive) to a Holo (active) conformation in response to low energy metabolite concentration, i.e., increased P_i or reduced PCr or ATP [75–77]. This feature would provide a protective network-inhibition mechanism when energy demands exceed metabolic capacities. Furthermore, our present work also shows that GABAergic markers (*Gad1*, *Gad2* and *Pvalb*) were highly correlated with the animals' behavior (Fig. 5D–F). Considering that fast-spiking parvalbumin-positive interneurons, particularly activated during gamma-oscillations in the hippocampus, are known to be very energy consuming and mitochondria-rich [78], improving energy metabolism might confer significant resilience to this cell population in particular. Of note, Uchida et al. reported that disruption of *Gad1* function can lead to the loss of parvalbumin neurons in the hippocampus as a result of stress exposure [79]. Interestingly, several studies have also reported lower post-mortem levels of *Gad1* expression in PFC of bipolar and schizophrenic patients [80–84]. Importantly, and of potential therapeutic relevance, ebselen was able to rescue the behavior in *Crtc1*$^{-/-}$ mice, by restoring hippocampal energy metabolites and levels of *Gad2* and *Pvalb* expression (Fig. 4). This resonates with previous reports of increased GABA metabolism enzymes expression in hippocampus after ebselen treatment [85]. Given its synaptic location and dynamic regulation, *Gad2*, encoding the GAD65 isoform, is likely to play a critical role in linking metabolic with electrophysiological activity (Fig. 5D, E). While it remains to be tested whether relative GAD conformation was altered and whether the rise in neurotransmitter cycling affected electrical activity in *Crtc1*$^{-/-}$ mice, we speculate that the low P_i and PCr observed must create a shift from Apo- to Holo-GAD, which would drive a compensatory drop in mRNA level, as observed here, allowing this enzyme to maintain a stable rate of GABA synthesis (Fig. 5G). This process would in turn favor the recycling of GABA for and from inhibitory neurotransmission rather than synthesis from glutamate, providing a mechanism to avoid excessive energy expenditure coming from extra metabolic steps, particularly when energy resources are low (Fig. 6). Although it is clear that Parvalbumin neurons are involved in this process, future mechanistic studies should address whether changes in Pvalb expression reflect differences in signaling within these neurons, such as involving BDNF-TrkB [86], or actual loss of neurons. Importantly, parvalbumin interneurons have been reported to be devoid of CRTC1 [19], suggesting that their dysfunction might not be directly related to *Crtc1* deletion. Moreover, it is important to note that glial fluxes were assumed to be similar between our groups, due to the technical limitations of [U-$^{13}C_6$]-glucose in distinguishing astrocytic contribution. Although it is known that CRTC1 is present in astrocytes [87], the consequences of its depletion in these cells remain to be identified. Nevertheless, with our current model, an increase (although not significant) in Gln exchange flux between two astroglial pools was observed, providing new avenues for understanding the role of glial cells. For instance, future experiment using ^{13}C substrate will provide further insight into the implication of astrocytes in *Crtc1*-related hippocampal energy imbalance [88].

With the help of neuroimaging technologies such as MRS, MRI and PET we have identified potential clinically relevant biological markers with their associated environmental dependences, opening potential therapeutic strategies. Using high-field ^{1}H-MRS we observed a drop in energy metabolites PCr and lactate in the hippocampus (Fig. 1) that were associated with depressive-like behavior (Fig. 3), suggesting their potential use as psychopathological "state" markers. While both metabolites were found to be

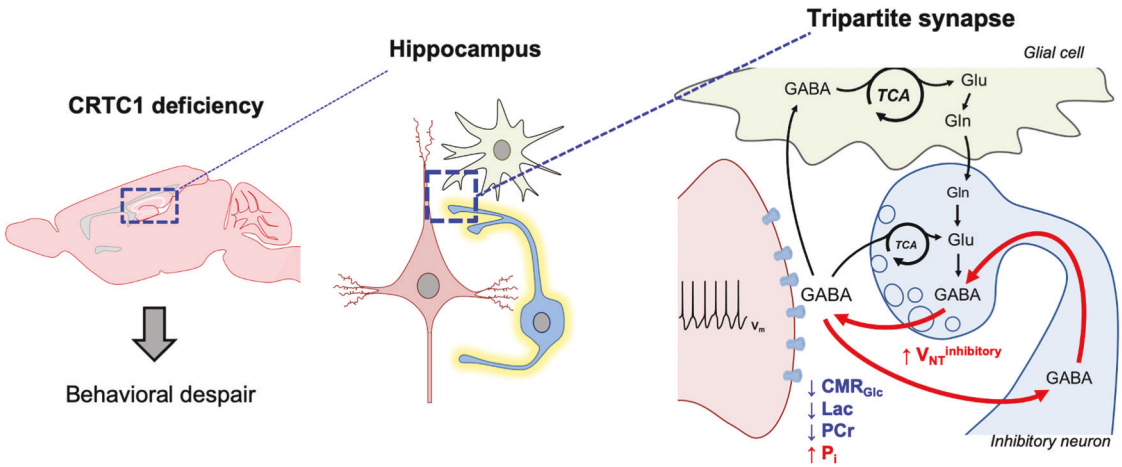

Fig. 6 Scheme of hippocampal GABAergic hyperactivity resulting from low energetic status linking *Crtc1* deletion to depressive-like behavior. Reduced hippocampal glucose metabolism capacity relative to neuronal neurotransmitter cycling-demands leads to low energetic status (high inorganic phosphate (P_i) and low phosphocreatine (PCr) levels) in *Crtc1* deficient mice. This results in excessive GABAergic neurotransmitter cycling and depressive-like behavior.

lower in *Crtc1*$^{-/-}$ mice under basal conditions (i.e., 6 weeks of age; Figs. 1, 3C and 4C) and associated with reduced glucose uptake measured with PET (Fig. 2A–D), the addition of an external stressor (social isolation or OSFST) was able to modulate both the behavior and these in vivo markers (Figs. 3 and 4). Stress, by challenging brain energetics, was shown to impact brain PCr content and behavior in chronic social defeat or chronic restraint protocols in mice [53, 56]. Social isolation is known to affect the behavior in other rodents as well [89–91] and induces several biological dysfunctions such as oxidative damage [92], a loss of hippocampal parvalbumin neurons [93] or drop in PCr content [94, 95]. Accordingly, PCr and lactate levels appeared to relate tightly to the level of stress experienced and stimulating mitochondrial metabolism with ebselen was able to restore normal PCr levels together with normal behavior (Fig. 4). Of note, *Crtc1*$^{-/-}$ mice are very aggressive and show altered social behavior [30], thus rendering group housing more stressful for them than social isolation, which would explain the opposite behavioral and neurometabolic response observed compared to WT mice. Importantly, an effect of ageing might also have contributed to the observed phenotype. Nevertheless, low lactate concentration, which can indicate both low glycolytic activity or high mitochondrial function, requires further considerations if it is to be indicative of a brain energetic status-based pathological state marker by itself. As such, hippocampal energy metabolite concentration showed a moderate ability to distinguish mice with "high" and "low" depressive-like behavior (Fig. S4F). Nevertheless, developing refined neuroimaging markers or functional paradigms to measure hippocampal neuroenergetics may allow significant clinical applications in the future. Furthermore, by combining MRI morphological analysis and ^{1}H-MRS, we have identified putative inflammatory markers in the cingulate cortex (Figs. S2B, S3 and S5A–C) that did not relate to the behavioral status, but reflected mouse genetic "susceptibility". Specifically, we have been able to consistently observe an increase in prefrontal tCho, or specifically GPC and PCho, the degradation product and precursor of phosphatidylcholine (PtdCho) respectively, in *Crtc1*$^{-/-}$ mice, together with PFC volume increase. Importantly, tCho concentration and tissue volume in PFC was able to differentiate *Crtc1*$^{-/-}$ from WT mice (AUC: 82%), suggesting a potential use for clinical diagnosis or predicting treatment-compatibility. Interestingly, several MRS studies have reported elevated tCho levels in the anterior cingulate cortex of patients with bipolar disorders [96–99] and these metabolites have been previously used as a MRS biomarker, such as for diagnostic of neoplastic tumor lesions in the brain [100–103]. Future research should address whether our observations in the DH and PFC could serve, respectively, as potential "diagnostic" and "predictive" clinical biomarkers for MD. Finally, by identifying how in vivo brain markers associated with *Crtc1* respond to the environment, we provide a better characterization and understanding of the factors that influence the path from gene to depressive-like behavior, providing a hopeful step forward toward a precision medicine-based approach in the field of psychiatry.

REFERENCES

1. Friedrich MJ. Depression is the leading cause of disability around the world. JAMA. 2017;317:1517. http://jama.jamanetwork.com/article.aspx?doi=10.1001/jama.2017.3826.
2. Mathers C, Fat DM, Boerma JT The global burden of disease: 2004 update. Geneva: World Health Organization; 2008.
3. Li X, Frye MA, Shelton RC. Review of pharmacological treatment in mood disorders and future directions for drug development. Neuropsychopharmacology. 2012;37:77–101. https://doi.org/10.1038/npp.2011.198.
4. Lenzenweger MF. Endophenotype, intermediate phenotype, biomarker: definitions, concept comparisons, clarifications. Depress Anxiety. 2013;30:185–9.
5. Hasler G, Northoff G. Discovering imaging endophenotypes for major depression. Mol Psychiatry. 2011;16:604–19. https://doi.org/10.1038/mp.2011.23.
6. Abi-Dargham A, Horga G. The search for imaging biomarkers in psychiatric disorders. Nat Med. 2016;22:1248–55. http://www.nature.com/articles/nm.4190.
7. Marazziti D, Rutigliano G, Baroni S, Landi P, Dell'Osso L. Metabolic syndrome and major depression. CNS Spectr. 2014;19:293–304.
8. Nasca C, Watson K, Bigio B, Robakis T, Myoraku A, Wroolie T, et al. Childhood trauma and insulin resistance in patients suffering from depressive disorders. Exp Neurol. 2019;315:15–20. https://linkinghub.elsevier.com/retrieve/pii/S0014488618304540; http://www.ncbi.nlm.nih.gov/pubmed/30639184.
9. Watson K, Nasca C, Aasly L, McEwen B, Rasgon N. Insulin resistance, an unmasked culprit in depressive disorders: promises for interventions. Neuropharmacology 2018;136:327–34.
10. Rasgon NL, McEwen BS. Insulin resistance—a missing link no more. Mol Psychiatry. 2016;21:1648–52.
11. Quteineh L, Preisig M, Rivera M, Milaneschi Y, Castelao E, Gholam-Rezaee M, et al. Association of CRTC1 polymorphisms with obesity markers in subjects from the general population with lifetime depression. J Affect Disord. 2016;198:43–9. https://doi.org/10.1016/j.jad.2016.03.031.
12. Choong E, Quteineh L, Cardinaux J-R, Gholam-Rezaee M, Vandenberghe F, Dobrinas M, et al. Influence of CRTC1 polymorphisms on body mass index and fat mass in psychiatric patients and the general adult population. JAMA Psychiatry. 2013;70:1011–9. http://archpsyc.jamanetwork.com/article.aspx?doi=10.1001/jamapsychiatry.2013.187.
13. Lu Y, Day FR, Gustafsson S, Buchkovich ML, Na J, Bataille V, et al. New loci for body fat percentage reveal link between adiposity and cardiometabolic disease risk. Nat Commun. 2016;7:10495. http://www.nature.com/articles/ncomms10495.

14. Delacrétaz A, Glatard A, Dubath C, Gholam-Rezaee M, Sanchez-Mut JV, Gräff J, et al. Psychotropic drug-induced genetic-epigenetic modulation of CRTC1 gene is associated with early weight gain in a prospective study of psychiatric patients. Clin Epigenetics. 2019;11:198. https://clinicalepigeneticsjournal.biomedcentral.com/articles/10.1186/s13148-019-0792-0.
15. Alisch RS, Van Hulle C, Chopra P, Bhattacharyya A, Zhang S, Davidson RJ, et al. A multi-dimensional characterization of anxiety in monozygotic twin pairs reveals susceptibility loci in humans. Transl Psychiatry. 2017;7:1282. http://www.nature.com/articles/s41398-017-0047-9.
16. Saura CA, Cardinaux J. Emerging roles of CREB-regulated transcription coactivators in brain physiology and pathology. Trends Neurosci. 2017;40:720–33. https://doi.org/10.1016/j.tins.2017.10.002.
17. Uchida S, Shumyatsky GP. Synaptically localized transcriptional regulators in memory formation. Neuroscience. 2018;370:4–13. https://linkinghub.elsevier.com/retrieve/pii/S0306452217304931.
18. Kovács KA, Steullet P, Steinmann M, Do KQ, Magistretti PJ, Halfon O, et al. TORC1 is a calcium- and cAMP-sensitive coincidence detector involved in hippocampal long-term synaptic plasticity. Proc Natl Acad Sci USA. 2007;104:4700–5. http://www.ncbi.nlm.nih.gov/pubmed/17360587.
19. Sekeres MJ, Mercaldo V, Richards B, Sargin D, Mahadevan V, Woodin MA, et al. Increasing CRTC1 function in the DentaGyrus during memory formation or reactivation increases memory strength without compromising memory quality. J Neurosci. 2012;32:17857–68. http://www.jneurosci.org/cgi/doi/10.1523/JNEUROSCI.1419-12.2012.
20. Nonaka M, Kim R, Fukushima H, Sasaki K, Suzuki K, Okamura M, et al. Region-specific activation of CRTC1-CREB signaling mediates long-term fear memory. Neuron 2014;84:92–106. https://doi.org/10.1016/j.neuron.2014.08.049.
21. Rossetti C, Sciarra D, Petit J, Eap CB, Halfon O, Magistretti PJ, et al. Gender-specific alteration of energy balance and circadian locomotor activity in the Crtc1 knockout mouse model of depression. Transl Psychiatry. 2017;7:1269. http://www.nature.com/articles/s41398-017-0023-4.
22. Altarejos JY, Goebel N, Conkright MD, Inoue H, Xie J, Arias CM, et al. The Creb1 coactivator Crtc1 is required for energy balance and fertility. Nat Med. 2008;14:1112–7. http://www.nature.com/articles/nm.1866.
23. Meylan EM, Breuillaud L, Seredenina T, Magistretti PJ, Halfon O, Luthi-Carter R, et al. Involvement of the agmatinergic system in the depressive-like phenotype of the Crtc1 knockout mouse model of depression. Transl Psychiatry. 2016;6:e852. https://doi.org/10.1038/tp.2016.116.
24. Wang Y-J, Liu L, Wang Y, Wang J-L, Gao T-T, Wang H, et al. Imipramine exerts antidepressant-like effects in chronic stress models of depression by promoting CRTC1 expression in the mPFC. Brain Res Bull. 2020;164:257–68. https://doi.org/10.1016/j.brainresbull.2020.08.028.
25. Liu Y, Tang W, Ji C, Gu J, Chen Y, Huang J, et al. The selective SIK2 inhibitor ARN-3236 produces strong antidepressant-like efficacy in mice via the hippocampal CRTC1-CREB-BDNF pathway. Front Pharm. 2021;11:1–20. https://www.frontiersin.org/articles/10.3389/fphar.2020.624429/full.
26. Ni S, Huang H, He D, Chen H, Wang C, Zhao X, et al. Adeno-associated virus-mediated over-expression of CREB-regulated transcription coactivator 1 in the hippocampal dentate gyrus ameliorates lipopolysaccharide-induced depression-like behaviour in mice. J Neurochem. 2019:1–15. http://doi.wiley.com/10.1111/jnc.14670.
27. Jiang B, Wang H, Wang J-L, Wang Y-J, Zhu Q, Wang C-N, et al. Hippocampal salt-inducible kinase 2 plays a role in depression via the CREB-regulated transcription coactivator 1–cAMP response element binding–brain-derived neurotrophic factor pathway. Biol Psychiatry. 2018. http://www.ncbi.nlm.nih.gov/pubmed/30503507.
28. Breuillaud L, Halfon O, Magistretti PJ, Pralong FP, Cardinaux J. Mouse fertility is not dependent on the CREB coactivator Crtc1. Nat Med. 2009;15:989–90. http://www.nature.com/articles/nm0909-989.
29. Rossetti C, Cherix A, Guiraud LF, Cardinaux J-R. New insights into the pivotal role of CREB-regulated transcription coactivator 1 in depression and comorbid obesity. Front Mol Neurosci. 2022;15:1–18. https://www.frontiersin.org/articles/10.3389/fnmol.2022.810641/full.
30. Breuillaud L, Rossetti C, Meylan EM, Mérinat C, Halfon O, Magistretti PJ, et al. Deletion of CREB-regulated transcription coactivator 1 induces pathological aggression, depression-related behaviors, and neuroplasticity genes dysregulation in mice. Biol Psychiatry. 2012;72:528–36. https://doi.org/10.1016/j.biopsych.2012.04.011.
31. Meylan EM, Halfon O, Magistretti PJ, Cardinaux J-R. The HDAC inhibitor SAHA improves depressive-like behavior of CRTC1-deficient mice: possible relevance for treatment-resistant depression. Neuropharmacology. 2016;107:111–21. https://linkinghub.elsevier.com/retrieve/pii/S0028390816300843.
32. Gruetter R, Tkáč I. Field mapping without reference scan using asymmetric echo-planar techniques. Magn Reson Med. 2000;43:319–23.
33. Mlynárik V, Gambarota G, Frenkel H, Gruetter R. Localized short-echo-time proton MR spectroscopy with full signal-intensity acquisition. Magn Reson Med. 2006;56:965–70. http://doi.wiley.com/10.1002/mrm.21043.
34. Provencher SW. Automatic quantitation of localized in vivo 1H spectra with LCModel. NMR Biomed. 2001;14:260–4.
35. Öz G, Deelchand DK, Wijnen JP, Mlynárik V, Xin L, Mekle R, et al. Advanced single voxel 1 H magnetic resonance spectroscopy techniques in humans: experts' consensus recommendations. NMR Biomed. 2021;34:1–18. https://onlinelibrary.wiley.com/doi/10.1002/nbm.4236.
36. Folch J, Lees M, Sloane Stanley GH. A simple method for the isolation and purification of total lipides from animal tissues. J Biol Chem. 1957;226:497–509. http://www.ncbi.nlm.nih.gov/pubmed/13428781.
37. Cherix A, Brodier L, Poitry-Yamate C, Matter J-M, Gruetter R. The appearance of the Warburg effect in the developing avian eye characterized in ovo: how neurogenesis can remodel neuroenergetics. Investig Opthalmology Vis Sci. 2020;61:3. https://iovs.arvojournals.org/article.aspx?articleid=2766010.
38. Lanz B, Poitry-Yamate C, Gruetter R. Image-derived input function from the Vena Cava for 18F-FDG PET studies in rats and mice. J Nucl Med. 2014;55:1380–8. http://jnm.snmjournals.org/cgi/doi/10.2967/jnumed.113.127381.
39. Cherix A, Donati G, Lizarbe B, Lanz B, Poitry-Yamate C, Lei H, et al. Excitatory/inhibitory neuronal metabolic balance in mouse hippocampus upon infusion of [U- 13 C 6]glucose. J Cereb Blood Flow Metab. 2020;632:0271678X2091053. http://journals.sagepub.com/doi/10.1177/0271678X20910535.
40. Walsh RN, Cummins RA. The open-field test: a critical review. Psychol Bull. 1976;83:482–504. http://www.ncbi.nlm.nih.gov/pubmed/17582919.
41. Lizarbe B, Cherix A, Gruetter R. In vivo heteronuclear magnetic resonance spectroscopy. Methods Mol Biol. 2018;1718:169–87.
42. Lizarbe B, Lei H, Duarte JMN, Lanz B, Cherix A, Gruetter R. Feasibility of in vivo measurement of glucose metabolism in the mouse hypothalamus by 1 H-[13 C] MRS at 14.1T. Magn Reson Med. 2018;80:874–84. http://doi.wiley.com/10.1002/mrm.27129.
43. Xin L, Lanz B, Frenkel H, Gruetter R. BISEP-based, ultra-short TE 1 H–[13 C] NMR spectroscopy of the rat brain at 14.1 T. 2009. www.jstage.jst.go.jp/browse/islsm.
44. McEwen BS. Stress, adaptation, and disease. Allostasis and allostatic load. Ann N Y Acad Sci. 1998;840:33–44. http://www.ncbi.nlm.nih.gov/pubmed/9629234.
45. Sonnay S, Duarte JM, Just N, Gruetter R. Compartmentalised energy metabolism supporting glutamatergic neurotransmission in response to increased activity in the rat cerebral cortex: a 13 C MRS study in vivo at 14.1 T. J Cereb Blood Flow Metab. 2016;36:928–40. http://journals.sagepub.com/doi/10.1177/0271678X16629482.
46. Azad GK, Tomar RS. Ebselen, a promising antioxidant drug: mechanisms of action and targets of biological pathways. Mol Biol Rep. 2014;41:4865–79. http://link.springer.com/10.1007/s11033-014-3417-x.
47. Martin SA, Souder DC, Miller KN, Clark JP, Sagar AK, Eliceiri KW, et al. GSK3β regulates brain energy metabolism. Cell Rep. 2018;23:1922–31.e4. https://doi.org/10.1016/j.celrep.2018.04.045.
48. Singh N, Halliday AC, Thomas JM, Kuznetsova OV, Baldwin R, Woon ECY, et al. A safe lithium mimetic for bipolar disorder. Nat Commun. 2013;4:1332. http://www.nature.com/articles/ncomms2320.
49. Sharpley AL, Williams C, Holder AA, Godlewska BR, Singh N, Shanyinde M, et al. A phase 2a randomised, double-blind, placebo-controlled, parallel-group, add-on clinical trial of ebselen (SPI-1005) as a novel treatment for mania or hypomania. Psychopharmacology. 2020. http://link.springer.com/10.1007/s00213-020-05654-1.
50. Watts AG, Sanchez-Watts G, Liu Y, Aguilera G. The distribution of messenger RNAs encoding the three isoforms of the transducer of regulated cAMP responsive element binding protein activity in the rat forebrain. J Neuroendocrinol. 2011;23:754–66. http://doi.wiley.com/10.1111/j.1365-2826.2011.02178.x.
51. Burkewitz K, Morantte I, Weir HJM, Yeo R, Zhang Y, Huynh FK, et al. Neuronal CRTC-1 governs systemic mitochondrial metabolism and lifespan via a catecholamine signal. Cell 2015;160:842–55. https://doi.org/10.1016/j.cell.2015.02.004.
52. Cao X, Li L-P, Wang Q, Wu Q, Hu H-H, Zhang M, et al. Astrocyte-derived ATP modulates depressive-like behaviors. Nat Med. 2013;19:773–7. http://www.nature.com/articles/nm.3162.
53. Cherix A, Larrieu T, Grosse J, Rodrigues J, McEwen B, Nasca C, et al. Metabolic signature in nucleus accumbens for anti-depressant-like effects of acetyl-L-carnitine. Elife 2020;9:1–19. https://elifesciences.org/articles/50631.
54. Chen W-J, Du J-K, Hu X, Yu Q, Li D-X, Wang C-N, et al. Protective effects of resveratrol on mitochondrial function in the hippocampus improves inflammation-induced depressive-like behavior. Physiol Behav. 2017;182:54–61. https://linkinghub.elsevier.com/retrieve/pii/S0031938417303098.
55. Gong Q, Yan X-J, Lei F, Wang M-L, He L-L, Luo Y-Y, et al. Proteomic profiling of the neurons in mice with depressive-like behavior induced by corticosterone and the regulation of berberine: pivotal sites of oxidative phosphorylation. Mol

Brain. 2019;12:118. https://molecularbrain.biomedcentral.com/articles/10.1186/s13041-019-0518-4.
56. Larrieu T, Cherix A, Duque A, Rodrigues J, Lei H, Gruetter R, et al. Hierarchical status predicts behavioral vulnerability and nucleus accumbens metabolic profile following chronic social defeat stress. Curr Biol. 2017;27:2202–10.e4. https://linkinghub.elsevier.com/retrieve/pii/S0960982217307297.
57. Mueller PL, Pritchett CE, Wiechman TN, Zharikov A, Hajnal A. Antidepressant-like effects of insulin and IGF-1 are mediated by IGF-1 receptors in the brain. Brain Res Bull. 2018;143:27–35. https://doi.org/10.1016/j.brainresbull.2018.09.017.
58. Anderson RM, Barger JL, Edwards MG, Braun KH, O'Connor CE, Prolla TA, et al. Dynamic regulation of PGC-1α localization and turnover implicates mitochondrial adaptation in calorie restriction and the stress response. Aging Cell. 2008;7:101–11. http://doi.wiley.com/10.1111/j.1474-9726.2007.00357.x.
59. Michael LF, Wu Z, Cheatham RB, Puigserver P, Adelmant G, Lehman JJ, et al. Restoration of insulin-sensitive glucose transporter (GLUT4) gene expression in muscle cells by the transcriptional coactivator PGC-1. Proc Natl Acad Sci. 2001;98:3820–5. http://www.pnas.org/cgi/doi/10.1073/pnas.061035098.
60. Ryan KM, Patterson I, McLoughlin DM. Peroxisome proliferator-activated receptor gamma co-activator-1 alpha in depression and the response to electroconvulsive therapy. Psychol Med. 2018:1–10. https://www.cambridge.org/core/product/identifier/S0033291718002556/type/journal_article.
61. Geoffroy PA, Etain B, Lajnef M, Zerdazi E-H, Brichant-Petitjean C, Heilbronner U, et al. Circadian genes and lithium response in bipolar disorders: associations with PPARGC1A (PGC-1 α) and RORA. Genes Brain Behav. 2016;15:660–8. http://doi.wiley.com/10.1111/gbb.12306.
62. Zhao Q, Wu X, Yan S, Xie X, Fan Y, Zhang J, et al. The antidepressant-like effects of pioglitazone in a chronic mild stress mouse model are associated with PPARγ-mediated alteration of microglial activation phenotypes. J Neuroinflammation. 2016;13:259. http://jneuroinflammation.biomedcentral.com/articles/10.1186/s12974-016-0728-y.
63. Kemp DE, Schinagle M, Gao K, Conroy C, Ganocy SJ, Ismail-Beigi F, et al. PPAR-γ agonism as a modulator of mood: proof-of-concept for pioglitazone in bipolar depression. CNS Drugs. 2014;28:571–81. http://link.springer.com/10.1007/s40263-014-0158-2.
64. Sepanjnia K, Modabbernia A, Ashrafi M, Modabbernia M-J, Akhondzadeh S. Pioglitazone adjunctive therapy for moderate-to-severe major depressive disorder: randomized double-blind placebo-controlled trial. Neuropsychopharmacology. 2012;37:2093–100. http://www.nature.com/articles/npp201258.
65. Lin KW, Wroolie TE, Robakis T, Rasgon NL. Adjuvant pioglitazone for unremitted depression: clinical correlates of treatment response. Psychiatry Res. 2015;230:846–52. https://linkinghub.elsevier.com/retrieve/pii/S0165178115304959.
66. Rahnert JA, Zheng B, Hudson MB, Woodworth-Hobbs ME, Price SR. Glucocorticoids alter CRTC-CREB signaling in muscle cells: impact on PGC-1α expression and atrophy markers. PLoS ONE. 2016;11:e0159181. https://dx.plos.org/10.1371/journal.pone.0159181.
67. Detka J, Kurek A, Kucharczyk M, Głombik K, Basta-Kaim A, Kubera M, et al. Brain glucose metabolism in an animal model of depression. Neuroscience. 2015;295:198–208. https://linkinghub.elsevier.com/retrieve/pii/S0306452215002833.
68. Kato T, Takahashi S, Shioiri T, Murashita J, Hamakawa H, Inubushi T. Reduction of brain phosphocreatine in bipolar II disorder detected by phosphorus-31 magnetic resonance spectroscopy. J Affect Disord. 1994;31:125–33. https://linkinghub.elsevier.com/retrieve/pii/0165032794901163.
69. Yuksel C, Du F, Ravichandran C, Goldbach JR, Thida T, Lin P, et al. Abnormal high-energy phosphate molecule metabolism during regional brain activation in patients with bipolar disorder. Mol Psychiatry. 2015;20:1079–84. http://www.nature.com/articles/mp201513.
70. Bradley KAL, Mao X, Case JAC, Kang G, Shungu DC, Gabbay V. Increased ventricular cerebrospinal fluid lactate in depressed adolescents. Eur Psychiatry. 2016;32:1–8. https://doi.org/10.1016/j.eurpsy.2015.08.009.
71. Lyra E, Silva NM, Lam MP, Soares CN, Munoz DP, Milev R, et al. Insulin resistance as a shared pathogenic mechanism between depression and type 2 diabetes. Front Psychiatry. 2019;10. https://www.frontiersin.org/article/10.3389/fpsyt.2019.00057/full.
72. Picard M, McManus MJ, Gray JD, Nasca C, Moffat C, Kopinski PK, et al. Mitochondrial functions modulate neuroendocrine, metabolic, inflammatory, and transcriptional responses to acute psychological stress. Proc Natl Acad Sci USA. 2015;112:E6614–23. http://www.pnas.org/lookup/doi/10.1073/pnas.1515733112.
73. Picard M, McEwen BS, Epel ES, Sandi C. An energetic view of stress: focus on mitochondria. Front Neuroendocrinol. 2018;49:72–85. https://doi.org/10.1016/j.yfrne.2018.01.001.
74. Nasca C, Bigio B, Zelli D, de Angelis P, Lau T, Okamoto M, et al. Role of the astroglial glutamate exchanger xCT in ventral hippocampus in resilience to stress. Neuron. 2017;96:402–13.e5.
75. Petroff OAC. GABA and glutamate in the human brain. Neuroscientist. 2002;8:562–73.
76. Martin DL, Rimvall K. Regulation of gamma-aminobutyric acid synthesis in the brain. J Neurochem. 1993;60:395–407. http://doi.wiley.com/10.1111/j.1471-4159.1993.tb03165.x.
77. Kass I, Hoke DE, Costa MGS, Reboul CF, Porebski BT, Cowieson NP, et al. Cofactor-dependent conformational heterogeneity of GAD65 and its role in autoimmunity and neurotransmitter homeostasis. Proc Natl Acad Sci USA. 2014;111:E2524–9. http://www.ncbi.nlm.nih.gov/pubmed/24927554.
78. Kann O, Papageorgiou IE, Draguhn A. Highly energized inhibitory interneurons are a central element for information processing in cortical networks. J Cereb Blood Flow Metab. 2014;34:1270–82. https://doi.org/10.1038/jcbfm.2014.104.
79. Uchida T, Furukawa T, Iwata S, Yanagawa Y, Fukuda A. Selective loss of parvalbumin-positive GABAergic interneurons in the cerebral cortex of maternally stressed Gad1-heterozygous mouse offspring. Transl Psychiatry. 2014;4:e371. http://www.nature.com/articles/tp201413.
80. Fung SJ, Webster MJ, Sivagnanasundaram S, Duncan C, Elashoff M, Weickert CS. Expression of interneuron markers in the dorsolateral prefrontal cortex of the developing human and in schizophrenia. Am J Psychiatry. 2010;167:1479–88. http://psychiatryonline.org/doi/abs/10.1176/appi.ajp.2010.09060784.
81. Hashimoto T, Bazmi HH, Mirnics K, Wu Q, Sampson AR, Lewis DA. Conserved regional patterns of GABA-related transcript expression in the neocortex of subjects with schizophrenia. Am J Psychiatry. 2008;165:479–89. http://linkinghub.elsevier.com/retrieve/pii/S0014482706004265.
82. Guidotti A, Auta J, Davis JM, Gerevini VD, Dwivedi Y, Grayson DR, et al. Decrease in reelin and glutamic acid decarboxylase67 (GAD67) expression in schizophrenia and bipolar disorder. Arch Gen Psychiatry. 2000;57:1061. http://archpsyc.jamanetwork.com/article.aspx?doi=10.1001/archpsyc.57.11.1061.
83. Woo TUW, Walsh JP, Benes FM. Density of glutamic acid decarboxylase 67 messenger RNA-containing neurons that express the N-methyl-D-aspartate receptor subunit NR2A in the anterior cingulate cortex in schizophrenia and bipolar disorder. Arch Gen Psychiatry. 2004;61:649–57.
84. Steiner J, Brisch R, Schiltz K, Dobrowolny H, Mawrin C, Krzyżanowska M, et al. GABAergic system impairment in the hippocampus and superior temporal gyrus of patients with paranoid schizophrenia: a post-mortem study. Schizophr Res. 2016;177:10–7.
85. Seo JY, Lee CH, Cho JH, Choi JH, Yoo K-Y, Kim DW, et al. Neuroprotection of ebselen against ischemia/reperfusion injury involves GABA shunt enzymes. J Neurol Sci. 2009;285:88–94. https://doi.org/10.1016/j.jns.2009.05.029.
86. Patz S, Grabert J, Gorba T, Wirth MJ, Wahle P. Parvalbumin expression in visual cortical interneurons depends on neuronal activity and TrkB ligands during an early period of postnatal development. Cereb Cortex. 2004;14:342–51.
87. Carriba P, Pardo L, Parra-Damas A, Lichtenstein MP, Saura CA, Pujol A, et al. ATP and noradrenaline activate CREB in astrocytes via noncanonical Ca2+ and cyclic AMP independent pathways. Glia. 2012;60:1330–44. https://onlinelibrary.wiley.com/doi/10.1002/glia.22352.
88. Lai M, Gruetter R, Lanz B. Progress towards in vivo brain 13C-MRS in mice: metabolic flux analysis in small tissue volumes. Anal Biochem. 2017;529:229–44.
89. Brenes JC, Rodríguez O, Fornaguera J. Differential effect of environment enrichment and social isolation on depressive-like behavior, spontaneous activity and serotonin and norepinephrine concentration in prefrontal cortex and ventral striatum. Pharm Biochem Behav. 2008;89:85–93. https://linkinghub.elsevier.com/retrieve/pii/S0091305707003462.
90. Brenes Sáenz JC, Villagra OR, Fornaguera Trías J. Factor analysis of forced swimming test, sucrose preference test and open field test on enriched, social and isolated reared rats. Behav Brain Res. 2006;169:57–65. https://linkinghub.elsevier.com/retrieve/pii/S0166432805005383.
91. Wallace DL, Han M-H, Graham DL, Green TA, Vialou V, Iñiguez SD, et al. CREB regulation of nucleus accumbens excitability mediates social isolation-induced behavioral deficits. Nat Neurosci. 2009;12:200–9. http://www.ncbi.nlm.nih.gov/pubmed/15123501.
92. Haj-Mirzaian A, Amiri S, Amini-Khoei H, Rahimi-Balaei M, Kordjazy N, Olson CO, et al. Attenuation of oxidative and nitrosative stress in cortical area associates with antidepressant-like effects of tropisetron in male mice following social isolation stress. Brain Res Bull. 2016;124:150–63. https://doi.org/10.1016/j.brainresbull.2016.04.018.
93. Ueno H, Suemitsu S, Murakami S, Kitamura N, Wani K, Okamoto M, et al. Region-specific impairments in parvalbumin interneurons in social isolation-reared mice. Neuroscience 2017;359:196–208. https://doi.org/10.1016/j.neuroscience.2017.07.016.
94. Shao Y, Yan G, Xuan Y, Peng H, Huang Q-J, Wu R, et al. Chronic social isolation decreases glutamate and glutamine levels and induces oxidative stress in the rat hippocampus. Behav Brain Res. 2015;282:201–8. https://linkinghub.elsevier.com/retrieve/pii/S0166432815000091.
95. Burjanadze G, Dachanidze N, Kuchukashvili Z, Chachua M, Menabde K, Koshoridze NI. Investigation of brain creatine levels under the mental stress conditions. J Stress Physiol Biochem. 2016;12:5–14.

96. Cao B, Stanley JA, Selvaraj S, Mwangi B, Passos IC, Zunta-Soares GB, et al. Evidence of altered membrane phospholipid metabolism in the anterior cingulate cortex and striatum of patients with bipolar disorder I: a multi-voxel 1H MRS study. J Psychiatr Res. 2016;81:48–55. https://doi.org/10.1016/j.jpsychires.2016.06.006.
97. Kubo H, Nakataki M, Sumitani S, Iga J, Numata S, Kameoka N, et al. 1H-magnetic resonance spectroscopy study of glutamate-related abnormality in bipolar disorder. J Affect Disord. 2017;208:139–44. https://doi.org/10.1016/j.jad.2016.08.046.
98. Soeiro-de-Souza MG, Otaduy MCG, Machado-Vieira R, Moreno RA, Nery FG, Leite C, et al. Lithium-associated anterior cingulate neurometabolic profile in euthymic Bipolar I disorder: a 1H-MRS study. J Affect Disord. 2018;241:192–9. https://linkinghub.elsevier.com/retrieve/pii/S0165032718310759.
99. Galińska-Skok B, Małus A, Konarzewska B, Rogowska-Zach A, Milewski R, Tarasów E, et al. Choline compounds of the frontal lobe and temporal glutamatergic system in bipolar and schizophrenia proton magnetic resonance spectroscopy study. Dis Markers. 2018;2018:1–7. https://www.hindawi.com/journals/dm/2018/3654894/.
100. Norfray JF, Tomita T, Byrd SE, Ross BD, Berger PA, Miller RS. Clinical impact of MR spectroscopy when MR imaging is indeterminate for pediatric brain tumors. Am J Roentgenol. 1999;173:119–25. http://www.ncbi.nlm.nih.gov/pubmed/10397111.
101. Rand SD, Prost R, Haughton V, Mark L, Strainer J, Johansen J, et al. Accuracy of single-voxel proton MR spectroscopy in distinguishing neoplastic from non-neoplastic brain lesions. Am J Neuroradiol. 1997;18:1695–704. http://www.ncbi.nlm.nih.gov/pubmed/7502961.
102. Poptani H, Gupta RK, Roy R, Pandey R, Jain VK, Chhabra DK. Characterization of intracranial mass lesions with in vivo proton MR spectroscopy. Am J Neuroradiol. 1995;16:1593–603. http://www.ncbi.nlm.nih.gov/pubmed/7502961.
103. Astrakas LG, Zurakowski D, Tzika AA, Zarifi MK, Anthony DC, De Girolami U, et al. Noninvasive magnetic resonance spectroscopic imaging biomarkers to predict the clinical grade of pediatric brain tumors. Clin Cancer Res. 2004;10:8220–8. http://www.ncbi.nlm.nih.gov/pubmed/15623597.

ACKNOWLEDGEMENTS

We thank Mrs. Janika Hannen and Dr. Fulvio Magara of the Centre d'Etude du Comportement (CEC) for technical assistance with mouse hippocampus dissection. This study was supported financially by the Center for Biomedical Imaging (CIBM) of the University of Lausanne (UNIL), University of Geneva (UNIGE), Geneva University Hospital (HUG), Lausanne University Hospital (CHUV), Swiss Federal Institute of Technology (EPFL) and the Leenaards and Louis-Jeantet Foundations and the Swiss National Science Foundation (Grants 31003A_149983 to RG and 31003A_170126 to JRC).

AUTHOR CONTRIBUTIONS

AC and JRC designed the study. AC, CPY, BL, OZ and JG acquired and analyzed the data. AC, CPY, CS, RG and JRC interpreted the data. AC drafted the manuscript. All the authors assisted in revising the manuscript and approved the final version.

FUNDING

Open access funding provided by University of Lausanne.

COMPETING INTERESTS

The authors declare no competing interests.

ADDITIONAL INFORMATION

Supplementary information The online version contains supplementary material available at https://doi.org/10.1038/s41380-022-01791-5.

Correspondence and requests for materials should be addressed to Antoine Cherix or Jean-René Cardinaux.